Journal of Computer Science

Research Article

A Comprehensive Review of Medical Image Denoising: Techniques, Challenges, Applications and Future Directions

Mohit Sharma[1], Ayush Dogra[2], Anita Gupta[1], Bhawna Goyal[3] and Dawa Chyophel Lepcha[4]

[1]*Department of Allied Health Sciences, Chitkara School of Health Sciences, Chitkara University, Punjab-140401, India*
[2]*Department of ECE, Chitkara University Institute of Engineering and Technology, Chitkara University, Punjab, India*
[3]*Department of Engineering, Marwadi University Research Centre, Marwadi University, Rajkot, Gujarat, 360003, India*
[4]*Graduate Institute of Biomedical Informatics, College of Medical Science and Technology, Taipei Medical University, New Taipei, 235, Taiwan*

Article history
Received: 16-04-2025
Revised: 23-07-2025
Accepted: 28-07-2025

Corresponding Author:
Ayush Dogra
Department of ECE, Chitkara University Institute of Engineering and Technology, Chitkara University, Punjab, India
Email: ayush123456789@gmail.com

Abstract: The concept of noise reduction in medical images plays a vital role in improving image quality and accuracy associated with diagnosis, and facilitating reliable automated analysis. This survey presents a structured overview of medical image denoising, beginning with foundational definitions and noise models for modalities such as MRI and CT. We critically evaluate persistent gaps, including the limited generalizability of deep learning models and the lack of clinical validation frameworks while proposing future directions to bridge these gaps. Medical image denoising has evolved through three distinct eras such as traditional filtering and transform-domain methods, data-driven machine learning approaches, and modern deep learning architectures. This review presents a paradigm-centric analysis of these developments, categorizing methods by their underlying learning framework and clinical imaging modality. We highlight how Convolutional Neural Networks (CNNs) and vision transformers have surpassed classical techniques in preserving diagnostic features while reducing radiation dose. We explore commonly used benchmark datasets that support the development and evaluation of denoising algorithms emphasizing their importance in standardizing comparisons. The paper systematically evaluates the strengths of each paradigm through both quantitative metrics and clinical utility assessments. Experimental details and findings from key studies are summarized illustrating methodological effectiveness and real-world implications. The clinical applications of denoising methods are also highlighted demonstrating their utility in improving image interpretability, surgical planning, and reducing radiation dose. Despite advancements, challenges persist, including limited generalizability across imaging conditions, difficulty in acquiring clean ground truth data, and the computational demands of deep models. We also examine limitations in model transparency and the need for clinical validation. Recent trends, including self-supervised learning, hybrid models, and real-time applications, offer promising directions for future research. This review aims to guide researchers by providing a consolidated understanding of medical image denoising methodologies and their clinical significance.

Keywords: Medical Image Denoising, Noise Formation Model, Deep Learning, Medical Images, Evaluation Metrics, Medical Imaging, Vision Transformers

Introduction

Medical imaging has transformed current diagnostic practices by providing a non-invasive method to visualize anatomy and pathologies (Shung et al., 2012). Unfortunately, the quality of medical imaging obtained from Computed Tomography (CT), Magnetic Resonance Imaging (MRI), Ultrasound (US), or Positron Emission

Tomography (PET) is often negatively impacted by noise artifacts that occur during acquisition, transmission, or reconstruction (Sagheer and George, 2020; Wu et al., 2023). Noise manifests as CT graininess, US speckle, or Rician noise in MRI, interfering with visualizing small details, lowering the confidence of a diagnosis, or creating a misinterpretation that affects the identification of critical findings (Rudin et al., 1992; Wang et al., 2004). The issue of medical image denoising lies is suppressing noise while retrieving diagnostically relevant structures like edges, textures, and small lesions. Complicating this problem is the unique profile of the noise associated with each imaging modality (Aja-Fernandez et al., 2008). Some of the earliest denoising methods utilized classical filtering approaches with spatial-domain approaches, including Gaussian and median filters (Goyal et al., 2020) or transform-domain methods like wavelet thresholding (Donoho,1995). Although simple and effective, these strategies suffer from over-smoothing effects, and in some cases require manipulation of manual parameters, limiting generalizability. With the emergence of machine learning, denoising methods have shifted to data-adaptive methods, like dictionary learning (Aharon et al., 2006) and sparse coding, for noise modeling, which in some cases can rely on handcrafted features (Jiang et al., 2025; Dabov et al., 2007). The ultimate transformation was the introduction of deep learning specifically Convolutional Neural Networks (CNNs) (Zhang et al., 2017), denoising autoencoders (Vincent et al., 2008), and Generative Adversarial Networks (GANs) (Ledig et al., 2017), which demonstrated significant power in learning from data and developing complex noise distributions in real-time. Recent advances, such as vision transformers (Chen et al., 2021) and self-supervised methods (Laine et al., 2019), push the bounds of denoising through the ability to capture long-range dependencies (i.e., pixels at a significant distance) and reduce reliance on paired training data (Lepcha et al., 2023a; Goyal et al., 2024). Although major trends continue to emerge and evolve, key issues remain. Many deep learning models have shown limited generalizability across imaging protocols or institutions (Kidoh et al., 2020, Huang et al., 2024a), while other approaches required computational sacrifices, like prohibitive time-windows in a clinical workflow (Liang et al., 2021). Additionally, the black-box nature of deep networks raises concerns regarding interpretability and trust in the clinic (Santos et al., 2024).

This review provides the first systematic review that establishes a classification of denoising methods into three chronological stages: Traditional, machine learning, and deep learning, and explores implications of denoising in the context of the key clinical imaging modalities (CT, MRI, US, and PET). Performance is assessed through both quantitative metrics (e.g., PSNR, SSIM) and clinical value and utility, culminating in a discussion of future goals and emerging styles (federated learning (Chen et al., 2024) explainable AI) (Upadhyay et al., 2021) for overcoming barriers between technical or foundational development and clinical implementation of denoising. Collectively, this effort will help provide classification, critical evaluation, and guidance to researchers when evaluating and selecting appropriate denoising strategies for medical imaging problems. We comprehensively investigated and defined a timeline of denoising strategies used in medical imaging for both 2D and 3D imaging techniques, in the modalities of MRI, CT, ultrasound, and PET. Although we place an emphasis on methodologies that generalize to various anatomical sites (e.g. brain, abdomen, chest), we relate performance to modality-specific noise models and clinical questions. In general, the methods are not limited to specific anatomical types unless the original writing explicitly indicated as in the core questions (e.g. preserving edges in MRI or suppressing speckle in ultrasound) are often not limited to a specific anatomical region. Section 3 (Benchmark Datasets) and Section 7 (Clinical Applications) are examples of when datasets/uses would target a specific anatomical region (e.g. IXI for brain MRI, LoDoPaB-CT for abdominal scans) in showcasing a practical use case. Taxonomy of our study is presented in Fig. 1.

Background

Problem Definition and Terminology

Let $\mathrm{X} = \{x_i \in \mathbb{R}\}_{i=1}^{n}$ represent an image with noise containing n image cells, which is affected by a function related to degradation Φ, and let $\mathrm{Y} = \{y_i \in \mathbb{R}\}_{i=1}^{n}$ denote the denoised version (Izadi et al., 2023). The Φ for the i-the image cell is expressed as:

$$x_i = \Phi\left(y_i; \theta_\eta\right); \qquad \forall_i \in \{1,2,3..,n\} \tag{1}$$

Where θ_η denotes the parameter set related to the degradation function and the system associated with disturbance. Noise degradation is typically modelled as the sum of noise followed by pixel-to-pixel elimination to take care of saturation occurs with respect to sensors. Let η_i represent the value of disturbance for the $i^{\text{-th}}$ pixel, which is actually induced by light/capturing device. Consequently, the system of additive disturbance can be expressed as:

$$x_i = \Phi\left(y_i; \theta_\eta\right) = \mathrm{clip}(y_i + \eta_i); \qquad \forall_i \in \{1,2,3..,n\} \tag{2}$$

Let us assume the intensities based on the image cells are confined to the interval [0, 1], we establish that $\mathrm{clip}(y_i) = \min(\max(y_i, 0), 1)$. The objective of noise reduction of the image is to get Y from the data with noise X.

The deterioration function and noise characteristics are generally not known. Consequently, the approximate value of the converse function is taken as given below:

$$\hat{y}_i = \Phi^{-1}(x_i; \theta_\zeta); \qquad \forall_i \in \{1,2,3..,n\} \tag{3}$$

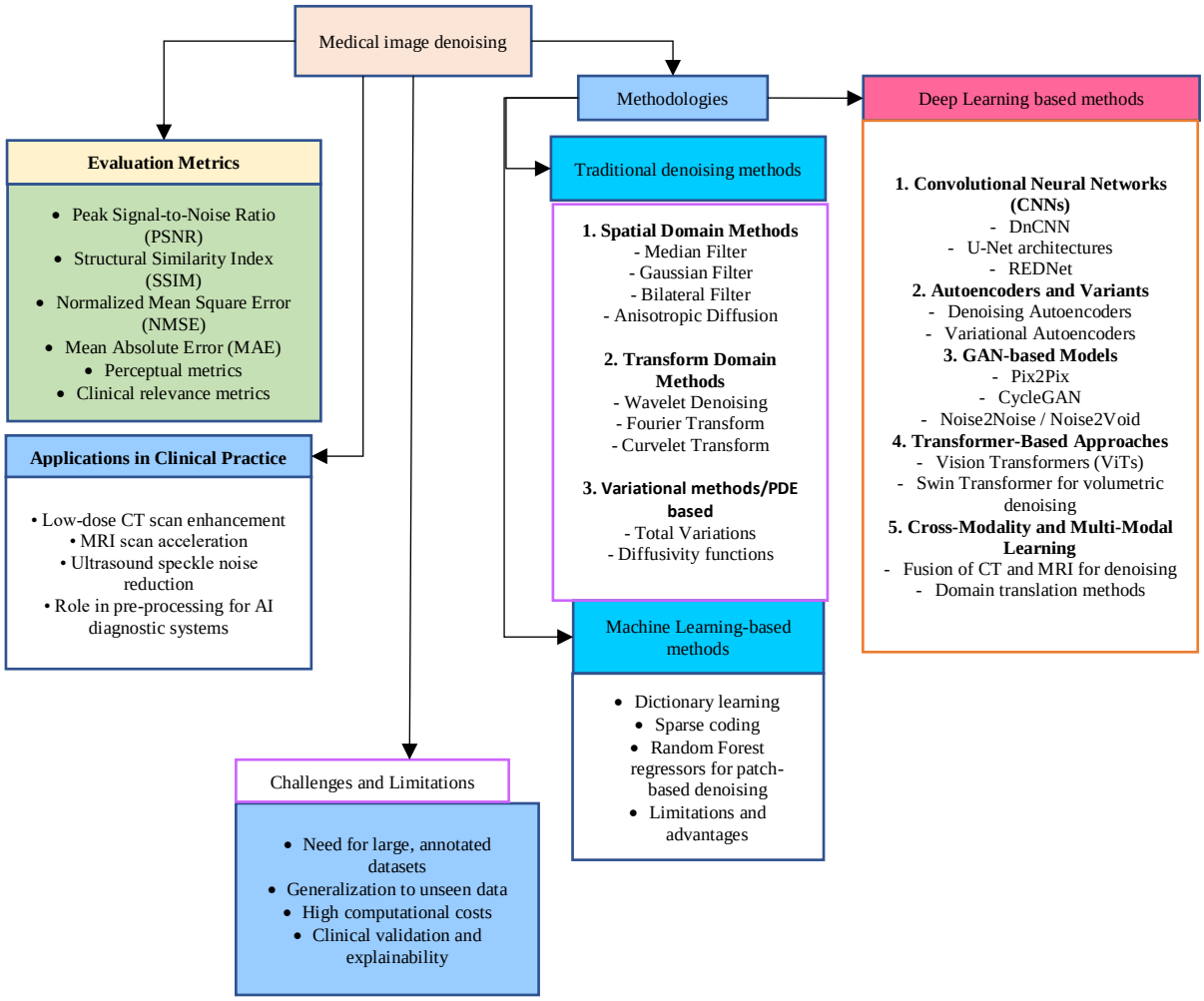

Fig. 1: Taxonomy of the medical image denoising

Where Φ^{-1} and θ_ζ represent the denoising function and its associated parameters, respectively. The learning-based denoiser functions as a regression model that correlates the noisy inputs X to the clean ground truth Y; specifically, $\Phi^{-1}: X \rightarrow Y$. In training a neural network as a denoiser, the loss generally consists of a fidelity term $\mathcal{L}(y_i, \hat{y}_i)$ that quantifies the difference between the clean estimate and the ground truth, along with a regularization term $\rho(\hat{y}_i)$ to constrain the solution, modulated by a variable λ. The set of connections based on denoising is instructed to acquire an ideal variable arrangement:

$$\theta^* = \arg\min_{\theta} \mathcal{L}(y_i, \hat{y}_i) + \lambda\, \rho(\hat{y}_i); \quad \in \{1,2,3..,n\} \tag{4}$$

While selecting fidelity, the aforementioned information of the input may be an imperative factor. The L2 distance fidelity term sometimes results in excessively smoothed outputs, potentially omitting high-frequency features due to the imposition of an output. Certain studies have shown that utilizing L1 distance yields superior image with restored eminence characterized by crisper corners etc. (Zhao et al., 2017).

Noise Formation Model

Noise in medical images results from complex, and modality-specific physical processes that occur when the data is acquired; thus, mathematical models must be developed to denoise medical images effectively. For instance, in CT imaging, noise is often assumed to be a hybrid Poisson-Gaussian distribution, arising from both quantum noise (photon statistics) and electronic readout noise (Liu et al., 2008; Foi et al., 2008). The heteroscedastic structure of CT noise can be represented using the following model:

$$x_i = y_i + \eta_i^{hg}, \qquad \eta_i^{hg} \sim \mathcal{N}(0, \alpha\, y_i + \sigma^2) \tag{5}$$

Where y_i is the noise-free pixel intensity, and α, σ^2 represent the signal-dependent and signal-independent components of noise, respectively (Donoho, 1995). MRI

noise, however is Rician-distributed; this arises because the complex-valued data are subjected to a magnitude reconstruction. The noise variance of MRI is proportional to the square-root of the signal (Aja-Fernandez et al., 2008):

$$x_i = \sqrt{\left(y_i - \eta_i^p\right)^2 + \left(\eta_i^q\right)^2}, \eta_i^p, \eta_i^q \sim \mathcal{N}(0, \sigma^2) \quad (6)$$

This nonlinearity biases low-intensity regions (e.g., background tissues), complicating denoising (Rabbani et al., 2009). Ultrasound exhibits speckle noise, a multiplicative artifact from coherent wave interference modelled as:

$$x_i = y_i . \eta_i^m + \eta_i^\alpha \quad (7)$$

Where η_i^m and η_i^α represent multiplicative and additive noise components (Benes and Riha, 2012). PET images suffer from Poisson noise as photons are counting limited and the noise variance equals the mean signal intensity per pixel (Thielemans et al., 2012). The varying characteristics of the noise specific to the medical imaging modalities apply to the design and concept of the denoising algorithm. Additive noise components such as electronic noise in CT, wavelet shrinkage methods (Naimi et al., 2015) and non-local means algorithms (Lu et al., 2012) are quite effective because they separate noise from signal in the transform domain or via patch based similarity metrics. Signal-dependent noise that is present in the MRI and PET imaging modalities do not have straightforward denoising strategies, since they rely on more complex methods such as variance-stabilizing transformations to stable the noise characteristics prior to applying processing, or deep learning methods (Geng et al., 2022) rely on the complex relationship between noise and signal learned from modality-specific training data. Ultrasound imaging has the unique challenge of speckle noise, and therefore, specialized techniques have been developed, such as Bayesian-optimized bilateral filtering (Taassori, 2024) that modify themselves to adapt to the local statistics of the image, and Generative Adversarial Networks (GANs) (Chen and Guo, 2023) which model and suppress the multiplicative patterns in noise and better preserve the tissue texture. The work discussed here demonstrates how noise modeling helps rationale algorithm selection or justification for modifications or adaptations to accommodate the noise characteristics found in each imaging modality. Recent attempts to advance the use of neural networks informed by physics have used these models as constraints on loss (Leuschner et al., 2019) and more recent self-supervised attempts (Krull et al., 2019) suggest an alternate approach of not modeling directly, but learning noise distributions directly from the corrupted data. Understanding the noise structure and mechanisms are essential to the iterative and improved clinical feedback loops for the denoising algorithms discussed.

Benchmarks Datasets

The chosen benchmark datasets for medical image denoising have the anatomical prioritization of each modality embedded in their designs. For example, brain MRI datasets (e.g., IXI, fastMRI) primarily care about preserving gray/white matter contrast, while abdominal CT datasets (e.g., Mayo Clinic, LoDoPaB-CT) care about reducing low-dose noise while preserving the boundaries of soft-tissue. The same can be seen in chest x-ray datasets (e.g., ChestX-ray14), which care about the visibility of lung pathology, and ultrasound datasets (e.g., PICMUS) which care about speckle suppression in vascular or cardiac structures. These anatomical distinctions are drivers in the design of datasets and the evaluation metrics adopted. There exist several datasets available on public platforms that contains variance in the characteristics like eminence, resolution, amount, diversity and most significantly the amount of noise and noise related attributes in them. In the section given below, we have reviewed a number of extensively used datasets with respect to the concept of denoising. The summary related to the above-mentioned datasets is presented in Table 1.

IXI Dataset: The IXI dataset comprises over 600 brain MRI scans from three hospitals in London, encompassing T1-weighted, T2-weighted, and Proton Density sequences. Although it lacks real noisy-clean image pairs, it is widely used for denoising research by introducing synthetic Rician or Gaussian noise. The dataset supports a variety of tasks such as segmentation, thanks to its multi-modality structure and diverse population sample ("IXI Dataset," https://brain-development.org/ixi-dataset/.).

fastMRI: Developed by NYU Langone Health and Facebook AI Research, the fastMRI dataset contains a huge corpus of raw k-space MRI related information and corresponding images for knee and brain scans acquired using 1.5T and 3T systems. It enables realistic noise simulation and has become a standard for benchmarking learning-based MRI reconstruction and denoising algorithms (Zbontar et al., 2018).

MRNet: The MRNet dataset, released by Stanford ML Group, contains MRI scans of the knee in three anatomical planes sagittal, coronal, and axial for over 1,300 studies. Although it was originally developed for abnormality classification, researchers often use it for denoising by synthetically injecting noise into clean scans (Bien et al., 2018).

Mayo Clinic Low-Dose CT Dataset: The Mayo dataset, part of the AAPM Low-Dose CT Grand Challenge, includes paired normal-dose and simulated low-dose abdominal CT scans. The low-dose images simulate realistic photon starvation noise, making this dataset essential for supervised deep learning-based CT denoising studies (Moen et al., 2021).

Table 1: Summary of Datasets

Sl. No.	Dataset Name	Modality	Paired (Noisy-Clean)	Noise Type	Dataset Details
1	IXI ("IXI Dataset," https://brain-development.org/ixi-dataset/.)	MRI (T1, T2, PD)	No	Synthetic (Rician)	Brain MRI: 600 scans from 3 London hospitals; widely used for neuroimaging denoising with artificial noise.
2	FastMRI (Zbontar et al., 2018)	MRI (Knee/Brain)	Raw data	Realistic (from k-space)	Knee/Brain MRI: Large-scale raw k-space data from NYU + Facebook AI; enables realistic noise modeling for musculoskeletal/neuro applications.
3	MRNet (Bien et al., 2018)	MRI (Knee)	No	Synthetic	Knee MRI: Sagittal/coronal/ axial views from 1,300+ studies; adapted for joint structure denoising.
4	Mayo Clinic Low-Dose CT (Moen et al., 2021)	CT (Abdomen)	Yes	Simulated (Poisson)	Abdominal CT: Paired normal/low-dose scans; essential for liver/kidney denoising in dose reduction studies.
5	LoDoPaB-CT (Leuschner et al., 2019)	CT	Yes	Simulated (Physics-based)	Thoracic/Abdominal CT: 40,000+ simulated low-dose slices; reference images for supervised lung/liver denoising.
6	NIH DeepLesion (Yan et al., 2018)	CT	No	Synthetic	Whole-body CT: 32,000+ axial slices with annotated lesions; repurposed for multi-organ noise reduction.
7	ChestX-ray14 (Wang et al., 2017)	X-ray (Chest)	No	Real (Clinical)	Chest X-ray: 112,000+ images with 14 pathology labels; focuses on lung denoising for pneumonia/TB detection.
8	JSRT ("JSRT Database," http://db.jsrt.or.jp/eng.php.)	X-ray (Chest)	No	Synthetic	Chest X-ray: 247 high-resolution images with lung masks; tests denoising for pulmonary structure preservation.
9	PICMUS ("PICMUS," https://www.creatis.insa-lyon.fr/Challenge/IEEE_IUS_2016/home.)	Ultrasound	Yes (RF data)	Real (Speckle)	Cardiac/General Ultrasound: Raw RF data for plane-wave imaging; targets speckle reduction in heart/vessels.
10	IVUS Challenge Dataset (Bernard et al., 2026; "Overview," https://www.creatis.insa-lyon.fr/Challenge/CETUS/.)	Intravascular US	Yes (paired frames)	Real (Speckle)	Coronary Ultrasound: Pullback sequences with arterial wall speckle for vascular denoising in cardiology.
11	STIR (Thielemans et al., 2012)	PET	(Simulated)	Simulated (Poisson)	Whole-body PET: Synthetic PET images with noise models applicable to oncology/neurology denoising.
12	MedNIST ("MedMNIST: Standardized Biomedical Images," https://www.kaggle.com/datasets/arashnic/standardized-biomedical-images-medmnist.)	Multi-modal	No	Synthetic	Multi-organ: Lightweight CT/MRI/X-ray/US images; synthetic noise tests across anatomical regions.

LoDoPaB-CT: LoDoPaB-CT, or the Low-Dose Parallel Beam CT dataset, consists of over 40,000 simulated low-dose CT images derived from LIDC-IDRI data, accompanied by noise-free references. This dataset is particularly useful for supervised and physics-informed deep learning approaches in CT denoising and sparse-view reconstruction (Leuschner et al., 2019).

NIH Deep Lesion: NIH Deep Lesion is a high scale public dataset of CT images featuring over 32,000 lesion-annotated slices from 10,000+ CT studies. While not designed specifically for denoising, it is commonly

repurposed by adding synthetic noise, and its clinical lesion annotations provide added value for downstream diagnostic performance evaluation (Yan et al., 2018).

ChestX-ray14: ChestX-ray14, released by the NIH, is one of the prevalent openly accessible datasets of radiography of chest, having more than 112,000 images with 14 pathology labels. It has become a common choice for no-reference or weakly-supervised denoising models, where researchers often apply artificial noise to emulate clinical noise scenarios (Wang et al., 2017).

JSRT: The JSRT dataset consists of 247 high-resolution chest X-rays, provided by the Japanese Society of Radiological Technology. While it does not contain noisy-clean pairs, its high-quality images and accompanying lung segmentation masks make it ideal for testing denoising algorithms using synthetic noise models Japanese Society of Radiological Technology (JSRT). (2026).

PICMUS: The PICMUS dataset was introduced as part of a beamforming challenge and provides Raw Radiofrequency (RF) data for plane wave ultrasound imaging. It is valuable for evaluating speckle denoising and coherence-based imaging techniques in ultrasound, where real-world acquisition data is scarce.

IVUS Challenge Dataset: The IVUS Challenge dataset includes intravascular ultrasound (IVUS) pullback sequences, capturing high-frequency speckle noise inherent to coronary imaging. It is primarily used for vessel wall segmentation, denoising, and texture analysis under realistic noise conditions found in cardiovascular imaging.

STIR: STIR (Software for Tomographic Image Reconstruction) is an open-source toolkit for simulating and reconstructing PET and SPECT images from synthetic or real sinogram data. It allows researchers to generate noisy-clean PET image pairs by modeling realistic Poisson noise and attenuation, supporting supervised denoising studies (Thielemans et al., 2012).

MedNIST: MedNIST is a lightweight, multi-modal dataset created for educational use in medical image classification, containing images from CT, MRI, X-ray, and ultrasound modalities. Due to its simplicity and structure, it has been widely adapted for denoising experiments through artificial noise injection across imaging domains (Yang and Shi, 2026).

State-of-the-Art Medical Image Denoising Methods

Medical image denoising is a critical preprocessing step focussed on upgrading the eminence of the image by decreasing the quantity of noise by retaining important anatomical details. From last few decades, numerous standard schemes have been created, starting from traditional filter-based techniques to advanced deep learning approaches. Recent trends emphasize convolutional and Generative Adversarial Neural networks (CNNs) and (GANs) and transformer-based architectures due to their superior performance in noise suppression and detail retention. These methods have significantly improved diagnostic accuracy in different modalities with respect to several kinds of medical images.

Traditional-Based Denoising Methods

Traditional denoising methods, which were designed prior to deep learning now remain the foundation of many projects due to their interpretation in a mathematical sense, and computational resources. They generally fit into one of three buckets of spatial-domain filters, transform-domain methods, and variational models, each with their own pros and cons in, depending on the image modality and corresponding noise accumulation. Wang et al. (2006) present a denoising algorithm for medical images that integrates total variation minimization with a wavelet approach. We demonstrate that our method provides efficient noise reduction in actual noisy medical photos while preserving object clarity. This technique enables the execution of an efficient automated criterion regarding the stopping time. Li and Que (2011) suggested denoising methods utilizing the differential of variation by examining the needs of imaging attributes from the perspective of image denoising, and employed the OpenCV platform for simulation. Luo et al. (2010) presented a method on the basis of spectrum data replacement system utilizing a numerical representation of one-dimensional singularity function analysis (1-D SFA). The scheme involves partitioning the entire spectral field related to noisy indicator into different divisions: The saved division, where the spectral information remains unmodified and the substitution division, where the actual information with the low value of SNR is changed with the redeveloped employing the 1-D SFA representation. Rabbani et al. (2009) introduced techniques for noise reduction to improve image quality across multiple modalities of images related to medical science, including MRI and multi-detector CT. The acquired 3-D data are initially processed using the discrete complex wavelet transform. They describe the data using a nonlinear function as the sum of the pristine information and Gaussian or Rayleigh noise. Fig. 2 depicts medical image denoising based on Kalman Bucy Filtered Neuro Fuzzy.

We employ a combination of bivariate Laplacian probability density functions for the pristine data in the modified area. Bhonsle et al. (2012) employed bilateral filtering for the noise reduction of images related to medical science.

The concept and implementation are straightforward, although the efficacy of the bilateral filter is contingent upon its parameters. (Benes and Riha, 2012) addresses the difficulty of speckle noise and its mitigation. Initially, the multiplicative speckle noise model and its mathematical representation are presented. Subsequently, specific de-noising techniques are delineated together with potential enhancements. An enhancement of the Kuan technique (KuanS) is offered based on their findings.

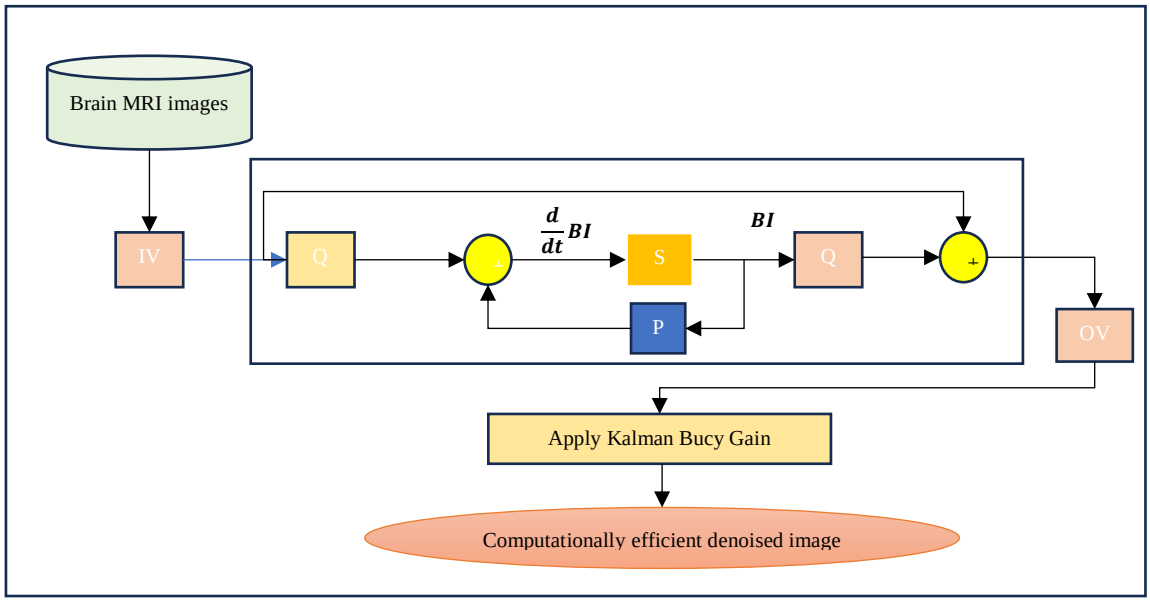

Fig. 2: Medical image denoising based on Kalman Bucy Filtered Neuro Fuzzy (Mohanapriya et al., 2026)

Lu et al. (2012) examine a hybrid methodology utilizing the patch NL-means design for the noise reduction of medical images. Unlike the conventional NL-means scheme which possesses some distinctive characteristics. Initially, we employ a constrained local neighbourhood to estimate the actual intensity of every denoised signal based on a selection of end-to-end image cells for the noise reduction procedure. The weights employed are determined based on the resemblance among the patch to be denoised and the different candidate patches. Ultimately, we utilize the kernel to maintain the details of the images. Sidhu et al. (2012) employ wavelet scheme to augment eminence of the image and reduce noise levels. It operates on Haar and Daubechies transforms. Initially, the image is deconstructed utilizing Haar and Daubechies transformations, followed by the selection of soft and hard threshold levels to mitigate noise in the image. Naimi et al. (2015) present a denoising method based on wavelet and shrinkage using dual tree, utilizing thresholding operational symbols of the complicated wavelet transform based on dual tree for noise reduction of medical images. The findings demonstrated that the images without noise utilizing DTCWT (Dual Tree Complex Wavelet Transform) exhibit superior equilibrium between smoothness and precision compared to DWT, while also being smaller duplicity than SWT (Stationary Wavelet Transform). Mohan et al. (2015) suggest a Multistage Median Filtering (MMF), an enhancement of the median filter that employs windows in all the directions. MMF gives spatial architectural attributes that effectively retain edges by distinguishing between flat and edge regions through the use of highest and lowest values. The outcome of MMF is assessed using each window and their combinations. Li et al. (2012) introduce an innovative dictionary learning technique, termed Dictionary Learning with Group Sparsity and Graph Regularization (DL-GSGR). The angular design of elements is represented through graph regularization. The DL-GSGR, which integrates group sparsity and graph regularization is addressed through the alternation of coding and updating related to dictionary. Fig. 3 shows Bayesian-optimized bilateral filtering for medical image denoising.

The consistency in groups of the modified dictionary can be sufficiently minimized to enable successful group sparse coding of any signal. Ultimately, group sparse representation utilizing DL-GSGR is employed for 3-D medical image denoising and image fusion. Bhadauria and Dewal (2013) propose a noise reduction technique for both Computed Tomography (CT) and Magnetic Resonance Imaging (MRI) that integrates images denoised by the Total Variation (TV) approach, denoised by a curvelet-based approach, and incorporates edge information, which is derived from the noise residual of the TV method processed with the help of curvelet transform. Satheesh and Prasad (2011) offer a medical image denoising approach utilizing contourlet transform. The results in mathematical form indicate that the given technique possesses a greater PSNR in comparison to the simple denoising schemes on the basis of wavelet scheme when implemented on the MR images under the existence of Additive White Gaussian Noise (AWGN).

Naimi et al. (2015) present a technique related to denoising based on the complex wavelet and shrinkage with dual tree by employing the Wiener filter with the use of different thresholding operational symbols of the DTCWT for the denoising of images related to medical science.

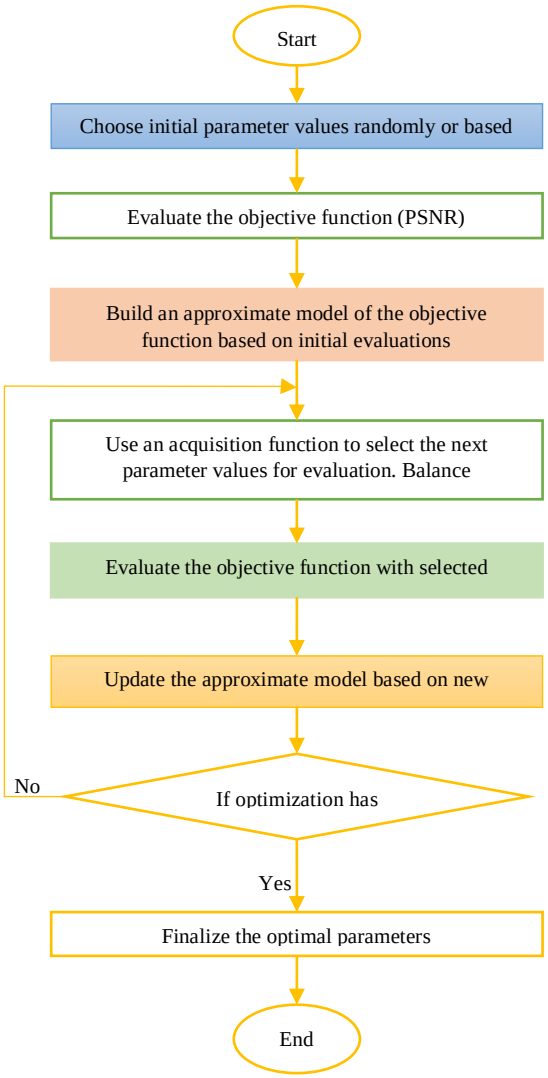

Fig. 3: Bayesian-optimized bilateral filtering for medical image denoising (Taassori, 2024)

Mingliang et al. (2016) enhance the kernel function with the weights specified in the NL-means technique for medical image denoising and introduce a GPU related concurrent non-local means scheme used for denoising. Zhao and Lu (2017) present an efficient model on variation for multimodal image fusion and denoising related to medical science. A multiscale alternating sequential filter is utilized to recover pertinent features from the medical images that possess noise. A recursive weight map based on the filtering approach is subsequently created to direct fusing of primary attributes from the images taken as input. Also, the TV constraint is formulated by creating an adaptive proportional command p that is contingent upon the contrast of the resultant image received after implementing fusion, so efficiently mitigating disturbance and preventing the zig-zag effect associated with TV. Cong-Hua et al. (2014) introduce a Generalized Gaussian Mixture Model (GGMM) using information about the corners for the noise reduction of images. In the initial phase, they enhance the Gaussian Mixture Model to the GGMM for representation of the noisy medical images and employ Minimum-Mean-Square Error (MMSE) inside the Bayesian structure to formulate a function related to non-linear mapping for the execution of these images with noise in them. In the subsequent phase, they enhance the outcomes utilizing the function based on kernel density of corners. Miri et al. (2018) present a novel method for eliminating Gaussian noise from the images employing the two-dimensional discrete cosine transform (2D-DCT) and the Ant Colony Optimization (ACO) algorithm. This approach aimed to uncover significant frequency coefficients through ant colony optimization while mitigating noise effects by eliminating high-frequency components. Anandan (2020) employ the Fast Discrete Curvelet Transform, a multi-scale geometric transformation intended to represent image or video sequences across many scales and orientations. Vaiyapuri et al. (2021) propose the improvement in functions related to multiple objectives for decreasing the disturbance from different images in the wavelet area. This shown scheme involves employing a Genetic Algorithm (GA) to sharpen the verge within the outline of reducing noise based on transform related to wavelet. Table 2 presents summary of traditional-based medical image denoising methods.

This technique serves two purposes: Firstly, it can adjust to various kinds of disturbance in the images without necessitating prior knowledge of the process of imaging itself. Kollem et al. (2021) offer an enhanced TV system created on Partial Differential Equations (PDE) that improves grey and colored brain tumor images acquired through MRI. A non-sub sampled contourlet transform was utilized on images from the approved databases, resulting in the conversion to lowpass and highpass also known as bandpass contourlet coefficients. An enhanced variant of the power law transformation technique was employed for the lowpass contourlet coefficients, while an accommodating scheme was utilized for the highpass contourlet coefficients. Benhassine et al. (2021) suggest an innovative method for image denoising utilizing DWT, emphasizing the choice of the optimal level with respect to decomposition and Haar wavelet. The function related to thresholding is subsequently applied to the coefficients taken in descriptive form. Optimal thresholding is achieved by novel improvement methods, including the crow search algorithm and social spider optimization approaches. The converse of the DWT is subsequently employed to rebuild the resultant image.

The suggested technique is assessed using the outcome evaluators like PSNR, SSIM and MSE etc. computation. Mohanapriya et al. (2026) propose a Kalman Bucy Filtered Neutrosophic Neuro Fuzzy Image Denoising (KBF-NNFID) technique aimed at minimizing noisy artifacts while upgrading the PSNR efficiently.

Table 2: Summary of Traditional-Based Medical Image Denoising Methods

Authors	Year	Methods	Detailed Findings
Kollem et al.	2021	Partial differential equation, non-subsampled contourlet transform	Improved method for decreasing the disturbance using partial differential equations combined with a non-subsampled contourlet transform.
Mohanapriya et al.	2026	Kalman Bucy Filter, Neuro Fuzzy	Denoising of medical images using a Kalman Bucy Filter in combination with neuro fuzzy techniques.
Benhassine et al.	2021	Optimal thresholding of wavelet coefficients	Wavelet-based thresholding for noise reduction with optimal selection of decomposition level and mother wavelet.
Taassori et al.	2024	Wavelet, Bayesian-Optimized Bilateral Filtering	Noise reduction approach based on wavelet enhanced by Bayesian-optimized bilateral filtering.
Taassori	2024	Edge-guided filtering, Fractional order total variation	CT denoising with edge-guided filtering using fractional order total variation.
Naimi et al.	2015	Dual tree complex thresholding, Wiener filter	Denoising using complicated thresholding wavelet transform with dual tree combined with a Wiener filter.
Mingliang et al.	2016	Parallel non-local means	Denoising medical images using parallel non-local means for improved performance.
Zhao et al.	2017	Alternating sequential filter, Adaptive fractional order total variation	A method for medical image fusion and denoising using alternating sequential filters and adaptive fractional order total variation.
Cong-Hua et al.	2014	Generalized Gaussian mixture modeling, Edge information	Denoising medical images using generalized Gaussian mixture modeling with edge information.
Anandan et al.	2020	Fast Discrete Curvelet Transform	Denoising medical images using the fast discrete curvelet transform.
Miri et al.	2018	2D discrete cosine transform, Ant colony optimization	Use of 2D discrete cosine transform in combination with ant colony optimization for medical image denoising.
Vaiyapuri et al.	2021	GA-based multi-objective optimization	Multi-objective optimization technique using genetic algorithms for medical image denoising in the wavelet domain.
Mohan et al.	2015	Multistage directional median filter	Multi-Stage Directional median filter in image noise reduction
Taassori and Vizvári	2024	Adaptive Kalman filter, non-local means, Latin Square Optimization	Hybrid denoising approach combining adaptive Kalman filter, non-local means, and Latin square optimization.

Initially, images associated with medical field from the Brain MRI LGG segmentation dataset undergo filtering using the Kalman-Bucy Filtering technique, with a sequence of quantities analyzed. Secondly, the resultant images serve as input, and ambiguity is addressed by the application of Neutrosophic Neuro Fuzzy Set (NNFS) utilizing the membership rank. Taassori (2024) introduces an improve technique on the basis of wavelet for reducing the noise in medical images designed to efficiently eliminate disturbance by maintaining essential image information. Subsequent to method of reducing noise with the help of wavelet, a bilateral filter is employed as a measure computed after the execution to further augment eminence of the image by diminishing noise and preserving sharpness at the edges. The efficiency of the bilateral filter is significantly contingent upon its parameters which require meticulous optimization. Diwakar et al. (2024) present a new function based on weights used with the fractional order TV helping in the blocky result as well as handling the non-convex issue related to the enhancement of images for better outcomes. Two different methodologies:

(i) Split Bregman
(ii) Augmented Lagrangian, were computed with the use of the suggested weighted fractional total variation denoising

Taassori and Vizvári, (2024) offer a new method designed to improve the scheme of decreasing noise effectiveness of images related to medical science. We first utilize a Kalman filter to reduce noise, capitalizing on its expertise in state estimation from contaminated observations. In contrast to traditional Kalman filters with static variables, our adaptive Kalman filter modifies its variables in response to the attributes of disturbance of the taken image hence providing improved precision in calculating approximately the accurate condition of the structure shown by the images based on medical field. Taassori (2024) introduces an advanced technique on the basis of wavelet for image related to the concept of denoising, designed to efficiently eliminate disturbance by maintaining essential image information. Following the process of reducing the noise using wavelet, a bilateral filter is employed as the execution after processing

measure to additionally improve eminence of an image. The efficacy of the bilateral filter is significantly contingent upon its parameters, which require meticulous optimization. We utilize Bayesian optimization, an effective method that proficiently determines the ideal filter settings, guaranteeing an improved equilibrium between the concept of decreasing the noise and retaining the details.

Deep Learning-Based Denoising Methods

Deep learning-based approaches have become the prevailing approach to medical image denoising due to their increased power of ability to model complex noise distribution, while recovering small contextual nuance in anatomical features. Among some of the most well-established architectures are Convolutional Neural Networks (CNNs), such as DnCNN, UNet, and REDNet, which attain good performance through the exploration of local spatial features, while maintaining the capacity to perform edge and texture preservation (Liu et al., 2019; Ming et al., 2020). Autoencoder-based approaches, from Denoising Autoencoders (DAEs) to Variational Autoencoders (VAEs) offer a complementary, unsupervised way of feature learning through encoding and reconstructing a noisy image (El-Shafai et al., 2022; Rawat et al., 2021) . In many cases, DAEs and VAEs can serve as baseline architectures in a more advanced processing pipeline. Generative Adversarial Networks (GANs), which include Pix2Pix, RED-CNN and CycleGAN have been utilized for both paired and unpaired denoising. GANs can produce perceptually plausible results; however, they can also produce synthetic textures that may need careful tuning for clinical applications (Zhou et al., 2020; Zeng et al., 2024; Li et al., 2021). Recent advances in Transformer-based architectures like the Swin Transformer and HCformer have shown improved performance by better capturing contextual information and long-range dependencies, and have re-validated the state of the art in denoising low-dose CT and volumetric MRI (Yuan et al., 2023; Jian et al., 2024). Additionally, hybrid and self-supervised methods such as Noise2Void, CNCL, and APNet overcome significant barriers such as the need for paired datasets and domain adaptation. These models have the capability to learn from unpaired images as well as images with only noise, and improve the practicality of translation to real-world clinical applications where clean ground truth images are often unavailable (Ledig et al., 2017; Geng et al., 2022). While evidence-based, particularly transformer-based, methods are highly effective, they are also computationally expensive, and require large and inclusive datasets for training. Translation into clinical practice will hinge on the availability of robust datasets, practical usability and operational fuel for explanatory and validated methods to be disseminated for clinical use. Leopard Seal Optimization (LSO) fine-tunes and optimizes the parameters of the network, assisting in improving the image denoising effect. The goal of image denoising in medical imaging is to meet a core need for clinical applications. The innovation of this research is the development of a MCVAN denoising model. The LSO optimization of the network parameters increases image denoising. Liu et al. (2019) propose a Genetic Algorithm (GA)-driven arrangement development scheme to identify the most suitable genes for the automatic optimization of network architectures. We accelerate the procedure based on evolution using a greedy investigation scheme and transfer learning. The said technique exhibits versatility, enabling the utilization of contemporary standard modules to explore prospective neural networks. Ming et al. (2020) present a Densely Connected Residual Network (DCRN) for the attenuation of disturbance in CT images related to low dose, integrating the concepts of dense connectivity. At one-point, dense connectivity optimizes transfer of information across layers associated with the network which is advantageous for preserving structural features during reduction of noise in images. Conversely, residual learning combined with batch normalization facilitates accelerated training and enhances noise reduction efficacy in images. Zhou et al. (2020) gave a system in relation to the supervised DL, CycleWGANs, to upgrading PET images in low dose. The tests related to validation were conducted on a dataset containing low-dose images derived from a genuine data containing lung cancer after biopsy or questionable radiological anomalies. Low dosage PET images were reconstructed from diminished PET images to achieve a calculation of 1 million. Conventional noise reduction techniques, specifically Non-Local Means (NLM) and Block-Matching 3D (BM3D), alongside 2 freshly published DL approaches, RED-CNN and 3D-cGAN, were incorporated for comparative analysis. Fig. 4 listed denoising framework for 2 stages deep denoising with self-guided noise attention.

Kim and Lee (2020) devise a technique of reducing the noise using DL for images of chest of the patients pertaining to low-dose, a frequently used procedure related to medical science for diagnostic purposes. Conditional Generative Adversarial Networks (CGANs) were employed in the formulation of the scheme based on decreasing the noise.

In order to train the system related to DL, we utilized the databases related to the SPIE American Association of Physicists in Medicine lung CT challenge with the Lung Image Database Consortium and Image Database Resource Initiative. Geng et al. (2022) suggest a straightforward yet efficacious approach, the plan based on the Content-Noise Complementary Learning (CNCL), wherein the predictors based on DL schemes were employed to understand the concept and the disturbance of the image information.

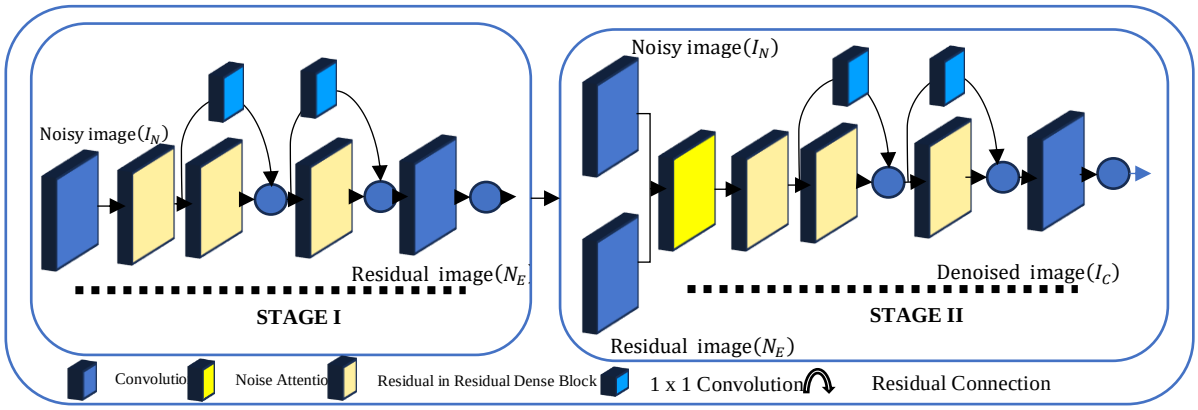

Fig. 4: Denoising framework for 2 stages deep denoising with self-guided noise attention (Sharif et al., 2024)

The noise reduction approach based on medical images utilizing the CNCL scheme is introduced, executed as a GAN, wherein multiple representative networks like U-Net are examined as the predictors used in the model. Rai et al. (2021) present an unsupervised technique for noise reduction approach based on medical images that acquires attributes with respect to noise from existing photos and generates resultant images without noise. It consists of two components related to the procedure of data execution named as patch-based dictionaries as well as Residual Learning (RL) that indirectly and directly learns the noise. The model is generalized to encompass both 2D and 3D images, taking into consideration various medical imaging devices. Luthra et al. (2021) introduces a transformer blocks arrangement for medical image noise reduction. The transformer block employs window-based attention which is not overlapped to decrease demands with respect to calculations. This study additionally integrates Sobel-Feldman operational symbols to augment edges of the images and suggests an efficient method for their concatenation inside the intermediate layers of the design. Zhang et al. (2017) provide anoise reduction scheme utilizing a Conditional Generative Adversarial Network (CGAN) to address diverse noise types. The suggested design integrates the image that has the disturbance with the matching gradient image as conditional fact related to the network, thereby augmenting the dissimilarity on the basis of architectural distinctiveness. A new generator utilizing residual dense blocks optimally leverages the interconnections among convolutional layers to investigate image. Additionally, the reconstruction loss and WGAN loss are amalgamated to form the objective loss function, ensuring the coherence between the resultant and the actual image. El-Shafai et al. 2022) propose the deployment of an automated detection model, referred to as CADTra, to effectively diagnose pneumonia-related conditions. This model utilizes categorization, denoising autoencoders, and transfer learning. The method relies on an Autoencoder Denoising (AD) design to enhance the likelihood of input recovery and effectively showcase their characteristics, hence improving the diagnostic process Sharif et al. (2020) mitigates the obstacles in the denoising operation by acquiring residual disturbance from a considerable volume of sample associated with the data. The suggested approach expedites the procedure of learning by implementing an innovative network that utilizes a structure leveraging attribute relation through the attention system, while integrating spatially refined residual features. Xu and Adalsteinsson (2021) present Deformed2Self integrates single-image and multi-image noise reduction to enhance eminence of the image and use a spatial set of connections to describe motion across many slices. Zhang et al. (2022) introduce a two-phase deep learning framework known as the Noisy Generation-Removal Network (NGRNet)Initially, the outputs from L0 Gradient Minimization serve as tags for a data available like dental CT images, creating false pairs of images with actual dental CT images, which are utilized to guide the set of connections associated with the creation of disturbance for estimating the genuine distribution. Rawat et al. (2021) introduce a novel model based on complicated CNN, referred to as CVMIDNet, which is examined for image disturbance reduction. Conversely, the conventional scheme that derives images without noise from disturbance exhibiting ones, the presented system uses RL to identify disturbance inside noisy images and subsequently minus it to yield clean images. Rajesh and Kumar (2022) formulated a Differential Evolution (DE) based system in this research to sharpen the designs of network and variables by identifying the most effective ones. Additionally, we employed learning with respect to transfer methodology to expedite the procedure related to training. The suggested scheme based on evolution is adaptable and identifies promising network designs utilizing established techniques. Fig. 5 illustrates Adversarial distortion learning for noise reduction.

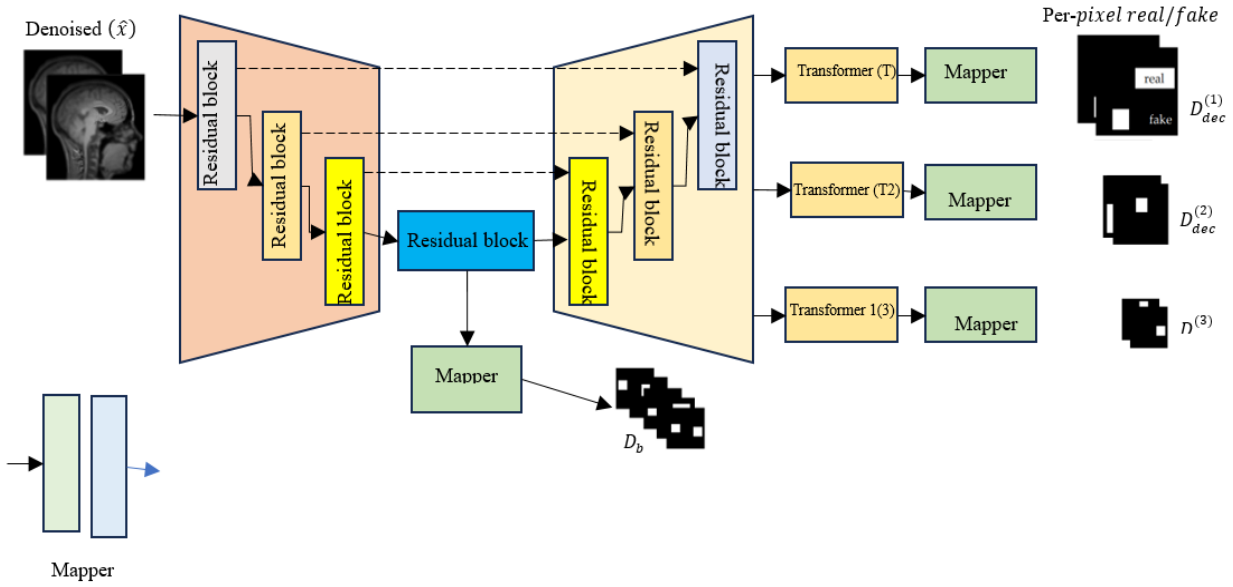

Fig. 5: Adversarial distortion learning for noise reduction (Ghahremani et al., 2022)

Kollem et al. (2022) introduce a novel method for image denoising that utilizes a partial differential equation on the basis on diffusivity function. This system utilizes a scheme named Quaternion Wavelet Transform to produce diverse coefficients based on disturbance, an enhanced generalized cross-validation function to determine the augmented threshold value and a novel diffusivity function to regulate the said procedure. Ghahremani et al. (2022) introduce an innovative Adversarial Distortion Learning (ADL) method for decreasing the disturbance of 2D/3D biological images. This scheme comprises of two auto-encoders: A denoiser and a discriminator. The denoiser eliminates disturbance from the input information, while the discriminator evaluates the output without noise against the equivalent that is without noise. Both the major components in the presented system are constructed using a suggested autoencoder known as Efficient-UNet. This system possesses a lightweight structural design which employs residual information as well as an innovative pyramid-like methodology at the back that effectively take out and reutilize feature maps. Singh et al. (2022-2023) presented a method to eradicate Gaussian white noise from CT images while maintaining intricate details. The suggested method integrates the idea of scheme noise using DL framework which utilizes a CNN. The damaged images are generated through the deliberate incorporation of Gaussian noise at several levels of noise (σ = 10, 15, 20, 25). Muksimova et al. (2023) provide a teacher student system that utilizes the capabilities of NoiseContextNet Block to identify and reduce noise maintaining exceptional accuracy. This modernization incorporates an iterative pruning strategy designed to enhance computing efficiency while maintaining the integrity of reducing noise. We exhibit the dominance and efficacy of the approach with the series of studies, highlighting substantial eminence improvements across various medical imaging modalities. Huang et al. (2024b) offer a sparse coding approach associated with self-supervision, called as the Weighted Iterative Shrinkage Thresholding Algorithm (WISTA). Conversely, to improve the efficacy of the method used, we spread out the WISTA to create a new WISTA on Deep Neural Network (DNN) structure which is named as WISTA-Net. Considering the pros of l_p-norm in the previous scheme, WISTA-Net demonstrates superior efficacy with respect to reducing the noise compared to the conventional Orthogonal Matching Pursuit (OMP) design and ISTA. Shivahare et al. (2023) introduced a notion wherein scheme disturbance is integrated with the structure created using deep learning for CNN, employing approach noise as a technique implemented after execution. Detecting brain tumors in noisy images poses significant challenges in achieving high accuracy. Therefore, this study presents a method for reducing the disturbance and identification of brain tumor utilizing CNN and U-Net. Table 3 summary of deep learning-based medical image denoising methods.

Diwakar et al. (2024) present a novel denoising methodology for Covid-19 CT images utilizing a CNN

and a noise-based thresholding approach. The primary focus of the approach is to mitigate the risks joined with the use of radiations during diagnostic procedures. The outcomes are assessed in the form of video through conventional outcome evaluators. The comparison revealed that the planned works yield superior results. (Jhang et al., 2024) introduced the Spach Transformer, an efficient spatial and channel-wise encoder-decoder transformer. Experiments utilizing datasets of various PET tracers, namely 18F-FDG, 18F-ACBC, 18F-DCFPyL, and 68Ga-DOTATATE, were performed to assess the suggested framework. (Yuan et al., 2023) introduced a hybrid CNN-Transformer (HCformer) codec network model for the denoising of LDCT images. A Neighbourhood Feature Enhancement (NEF) module is intended to include local information into the functioning of the Transformer, thereby augmenting the representation of neighboring pixel information in the LDCT image denoising process. The given method is employed to reduce the complexity of the system connections and address the challenges associated with calculating multi-head self-attention. Annavarapu and Borra (2024) proposed an adapted deep CNN for image disturbance reduction system which is subsequently enhanced with the incorporation of watershed segmentation on the basis of marker. The efficiency of the proposed scheme is assessed and evaluated on medical images that involves MRI and CT scans. Ferdi et al. (2024) propose an approach utilizing characteristic learning with respect to high-frequency to improve the process of decreasing noise efficacy of current systems. This approach aims to concurrently study the principal assignment of reducing the disturbance in LDCT images and the supplementary job of edge detection process on LDCT images that further leads to enhancing efficacy of decreasing the noise without augmenting model parameters or inference duration.

Zeng et al. (2024) present a Triplet Neural Networks Collaboration-Continuity Denoising (TNCDN) model. Employ triplet neural networks for cooperative mutual updates. The facts from these two networks related to denoising that possess progressive abilities associated with learning, is passed to the primary network based on denoising. This primary network possesses novel insights and can reinforce existing information. An assisted training system has been devised. Sharif et al. (2024) examine the shortcomings of current denoising techniques through an AI-driven two-stage learning approach. The said scheme acquires the capability to assess the residual disturbance from the contaminated images.

Table 3: Summary of Deep Learning-Based Medical Image Denoising Methods

Model Category	Methods	Core Techniques	Key Insights/Applications
CNN-Based Models	DnCNN (Liu et al., 2019), UNet (Shivahare et al., 2023), RED (Ferdi et al., 2024), DEN (Diwakar et al., 2024)	Convolutional layers, residual learning	Effective for structural preservation, fast inference, widely used in MRI & CT
Autoencoder-Based	DAE (El-Shafai et al., 2022), VAE (Rawat et al., 2021), Efficient-UNet (Ghahremani et al., 2022)	Encoding-decoding, feature compression	Unsupervised denoising, often used as backbone for other models
GAN-Based Models	CNCL (Geng et al., 2022), CycleGAN (Zhou et al., 2020), CGAN (Zhang et al., 2017), ADL (Ghahremani et al., 2022)	Adversarial training, perceptual realism	Excellent for low-dose imaging, can hallucinate artifacts if not tuned
Transformer/Hybrid	HCformer (Yuan et al., 2023), SwinCT (Swetha and Jyothi, 2025), APNet (Song et al., 2024), CT-ViT (Marcos et al., 2024)	Attention mechanism, CNN-Transformer fusion	Superior in handling global features, ideal for LDCT, 3D scans, high-noise environments
Self-Supervised & Noise-Aware	Noise2Void (Krull et al., 2019), CNCL (Zeng et al., 2024), WISTA-Net (Huang et al., 2024b), TNN (Zeng et al., 2024)	Noisy-only training, complementary learning	Useful where clean data is scarce, enables real-world deployment
Optimization/Meta-Learning	DE-based (Rajesh and kumar, 2022), GA-based (Miri et al., 2018), MCVAN (Jian et al., 2024)	Evolutionary search, attention fusion	Boost performance via architecture tuning and adaptive attention mechanisms

Subsequently, it integrates an innovative noise attention method to associate calculated residual disturbance with inputs with noise in them, facilitating disturbance reduction in a coarse-to-fine approach. This approach guides to utilize a multimodal learning technique to generalize reduction of noise across

categories of medical imaging and various noise patterns for extensive applicability. Marcos et al. (2024) presented a clean Vision Transformer (ViT) for decreasing the noise in artificial neural network focussed on execution of images based on medical science, especially in reducing the noise in the CT images pertaining to low dose. The suggested model adheres to a U-Net architecture incorporating ViT modules alongside the Noise2Neighbor (N2N) interpolation operation. This experiment utilized five distinct datasets comprising pairs of LDCT and normal-dose CT (NDCT) images. Song et al. (2024) devised an Adaptive Projection Network (APNet) to mitigate noise in low-dose medical images. APNet is constructed upon a **U**-shaped design of network to confine multi-scale information as well as smooth the progress of end-to-end denoising of images. A residual block of the dual attention approach is included throughout the encoding and decoding stages to adaptively calibrate significant aspects in information transmission. Jian et al. (2024) introduce SwinCT, an advanced model for the reduction of noise in LDCT images. SwinCT utilizes the Feature Enhancement Module (FEM) derived from Swin Transformer to extract and augment high-level features of medical images, while concurrently integrating with a deep noise reduction encoder-decoder network in the downstream task, thereby ensuring the retention of additional tissue and lesion details post-denoising. Swetha and Jyothi (2025) provide a Multilevel Convolutional Neural Network with an optimized Visual Attention Network (MCVAN) designed for image denoising to augment the value of PSNR. Leopard Seal Optimization (LSO) refines the network parameters, improving denoising efficacy. The objective is to fulfill the essential requirement for efficient image denoising in medical imaging. This research's innovation is the creation of a MCVAN designed for image denoising. The LSO's refinement of parameters further improves denoising efficacy.

Additionally, to facilitate more meaningful comparisons between denoising models Table 4 summarizes researchers evaluation of traditional, machine learning and clinical or original implementations across 4 critical categories; computational cost, data dependence, generalizability, and clinical readiness. Traditional techniques (e.g., Gaussian filters, wavelets) are computationally inexpensive, readily used and easy to operationalize; however, they may be limited in their ability to adapt, and to generalize with different noise types or anatomical structures. Machine learning methods, e.g. dictionary learning or sparse coding, improved adaptability with moderately sized datasets. Machine learning methods utilized handcrafted features, increasing pressure to vary, and mis-process about new regions outside "features". The deep learning model e.g. CNN-C, GAN, Transform, demonstrated the best performance as a processing capability by training representations directly from data, and all are highly computational/memory intensive requiring larger datasets. The clinical validation effort process is required prior to implementation due to data variability and representation. Deep learning, especially relevant to both capable explainable and domain adaptation self-supervised models, have emergent opportunity; and while complex deep learning methodologies will continuously evolve, the outlined deep learning models are not inherently developed nor refined for clinical practicality. This evaluation structure captures tradeoffs as they relate to algorithm selection, or models for development realization for effective image denoising for clinical applications.

Evaluation Metrics

Evaluating algorithms for denoising medical images is a multi-faceted process that includes a quantitative assessment along with clinical evaluations to ensure the algorithms are technically sound and have clinical relevance. Traditional full-reference metrics, such as Peak Signal-to-Noise Ratio (PSNR) (Lepcha et al., 2023b-c) and Structural Similarity Index (SSIM) (Goyal et al., 2020) remain prevalent as assessment metrics.

Table 4: Comparative evaluation of denoising approaches in medical imaging

Method	Techniques	Computational Cost	Data Dependency	Generalizability
Traditional	Gaussian filter, Wavelet, Bilateral filter	Low	None	Low modality/noise-type specific
ML-based	Dictionary learning, Sparse coding	Moderate	Moderate	Moderate; better than traditional but feature-engineered
Deep Learning	CNNs (DnCNN, UNet), GANs (Pix2Pix), ViTs	High	High	High adaptable across modalities, tasks
Hybrid/Transformers	APNet, HCformer, SwinCT	Very High	Very High	Very High; strong cross-domain transfer

PSNR calculates the absolute pixel-wise fidelity, while SSIM uses luminance, contrast and structure comparisons to provide an estimate of perceptual image quality. Both of these metrics, however, have limitations; PSNR tends to have a poor correlation with human perception, and SSIM does not always accurately account for small, diagnostic features (Lepcha et al., 2023b, d). To provide a more nuanced assessment, several feature-based metrics have gained popularity, including Feature Similarity Index (FSIM) and Natural Image Quality Evaluator (NIQE) (Goyal et al., 2024) Feature-based metrics hold some utility for analysis of denoising approaches across modalities, especially in ultrasound imaging where preservation of texture is important. In practice, no-reference metrics can be very useful (e.g., Blind/Referenceless Image Spatial Quality Evaluator (BRISQUE), Perception-based Image Quality Evaluator (PIQE) (Lepcha et al., 2023b-c) especially when there is not a clean image available to reference, allowing a practical utilization of an image quality assessment during image acquisition. In addition, task-specific evaluations, increasingly being seen as a parallel to traditional full-reference and no-reference metrics, are becoming more widely adopted, including studies on lesion detectability (Chen et al., 2017; Jacobs et al., 2021; Santos et al., 2024) and reader trials where radiologists measure diagnostic value instead of simple anesthetic improvements. Finally, deep learning applications are emerging that include other learned perceptual metrics such as Learned Perceptual Image Patch Similarity (LPIPS) (Li et al., 2025) that purport better correlation with human judgment by comparing deep feature representations. The determination of which evaluation framework to use is context-dependent: If PSNR/SSIM are useful for technical comparisons in artificially controlled studies (Ming et al., 2020), validation of low-dose CT requires radiation dosing quality tradeoff analysis (Chen et al., 2017; Jacobs et al., 2021), MRI denoising must maintain functional information in diffusion weighted sequences (Kang et al., 2024). The rapidly changing practice pattern of clinical imaging signifies the urgent need for standardized, modality-specific evaluation frameworks that allow for scientific rigor as well as clinical useful metrics which is currently being addressed by initiatives such as the AAPM Low-Dose CT Grand Challenge (Moen et al., 2021) and fastMRI benchmark (Zbontar et al., 2018). At the end of the day, the most important metric is whether the algorithm enhances diagnostic confidence while preserving anatomic and pathologic accuracy, ideally with multi-center clinical trials validating the later artifacts (Chu et al., 2017; Jacobs et al., 2021).

Experimental Details and Discussion

This segment evaluates the performance of the said denoising method using a number of experiments implemented on MRI datasets. The dataset used for these experiments is sourced from (https://www.med.harvard.edu/aanlib/home.html), an openly assessable repository extensively utilized in medical science research. The comparison is performed among well-known denoising techniques including FOTV (Diwakar et al., 2024), OD-CNN (Atal, 2023), NDiff (Kollem et al., 2023), SDPM (Gong et al., 2024), UDLF (Rai et al., 2021), NGN (Fu et al., 2022), CNCL (Geng et al., 2022), BP-MEC (Ji et al., 2020), FDCT (Anandan et al., 2020), BF-CNN (Elhoseny and Shankar, 2019), DEN (Liu et al., 2019), WT(Satapathy et al., 2019), DCT-ACO (Miri et al., 2018), NNE (Liu et al., 2018), SDL (Bai et al., 2018), TNN (Zeng et al., 2024), RED (Ferdi et al., 2024), AWS-DCNN (Annavarapu and Borra, 2024), AKF-NLM (Taassori and Vizvari, 2024), HCformer (Yuan et al., 2023), MCOVAN (Jian et al., 2024), APNet (Song et al., 2024), CNN-UNet (Shivahare et al., 2023), KBF (Mohanapriya et al., 2026), DE(Rajesh and Kumar, 2022), CDCRN (Ming et al., 2020), GA (Vaiyapuri et al., 2021), HSSD (Laine et al., 2019) and DTCT (Naimi et al., 2015). All methods are evaluated using their default parameters to ensure optimal performance and fair comparison. The evaluation includes three test images: two MRI scans (MRI1 and MRI2) selected from https://www.med.harvard.edu/aanlib/home.html. These images are tested under different levels (σ = 10,20,30 and 40) to assess robustness under different conditions. All experimentations were conducted using Matlab platform on a system with an Intel Core i5-4460 Quad Core processor 3.2 GHz and 16 GB of RAM. For performance evaluation, we employ seven widely standard image performance evaluators like PSNR, SSIM, FSIM, Entropy (Lepcha et al., 2023a-b), and three non-reference performance metrics such as BRISQUE, PIQE, and NIQE (Lepcha et al., 2023a-b). A higher value of PSNR, SSIM, FSIM, and Entropy (Goyal et al., 2024) represents better image quality performance, whereas lower BRISQUE, PIQE, and NIQE (Goyal et al., 2024) scores are desirable. The images used in the denoising experiments along with their visual and quantitative results are presented in Figures (6-8) and Tables (5-6). Figure 6 gives a video estimation of various noise reduction algorithms implemented to an MRI1 image with a noise level of $\sigma \approx 10$. The top-left image shows the noisy input, clearly affected by granular noise, which blurs anatomical structures and reduces diagnostic clarity.

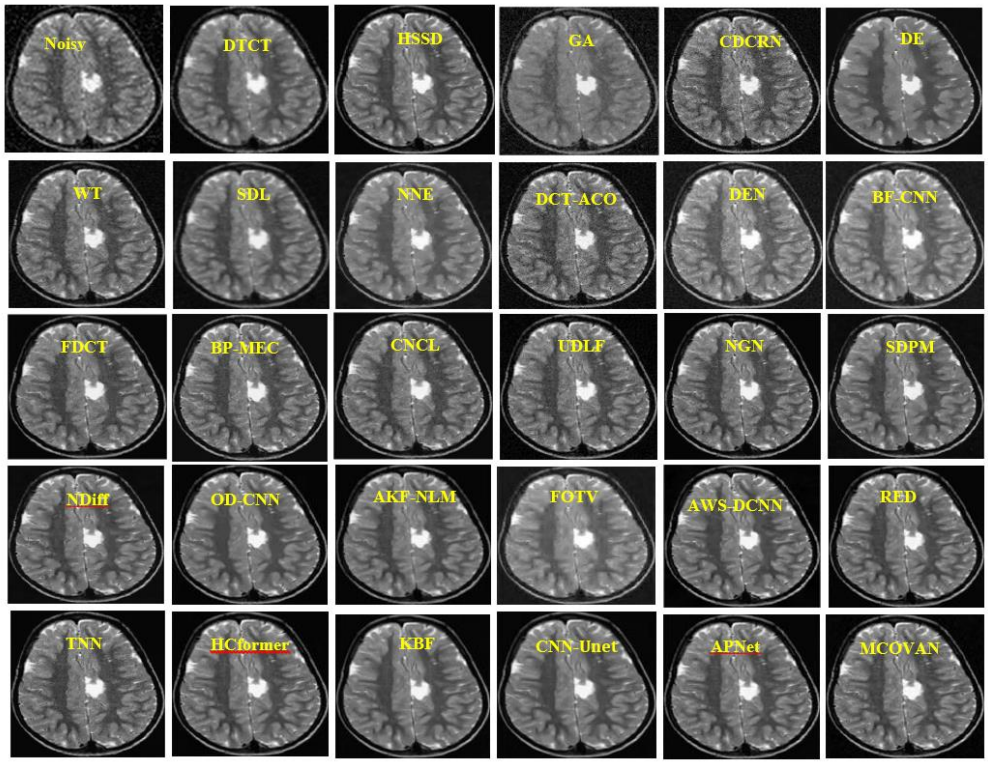

Fig. 6: Visual analysis of different standard noise reduction schemes on MRI1 image ($\sigma \approx 10$)

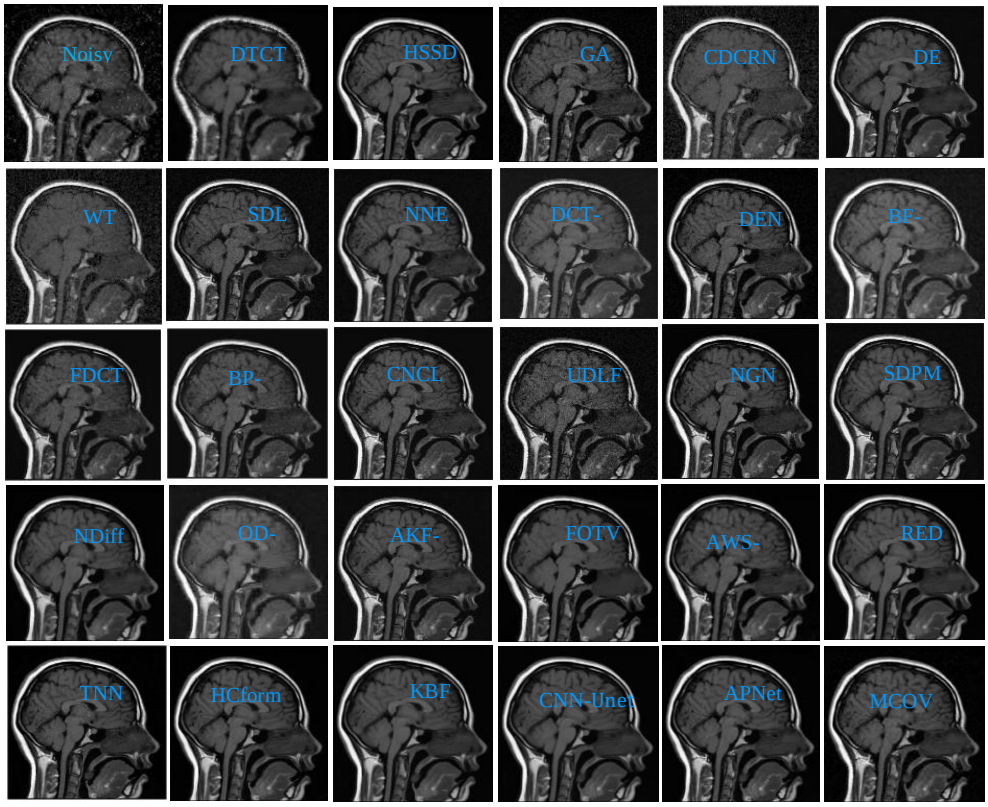

Fig. 7: Visual analysis of different standard noise reduction schemes on MRI2 image ($\sigma \approx 10$)

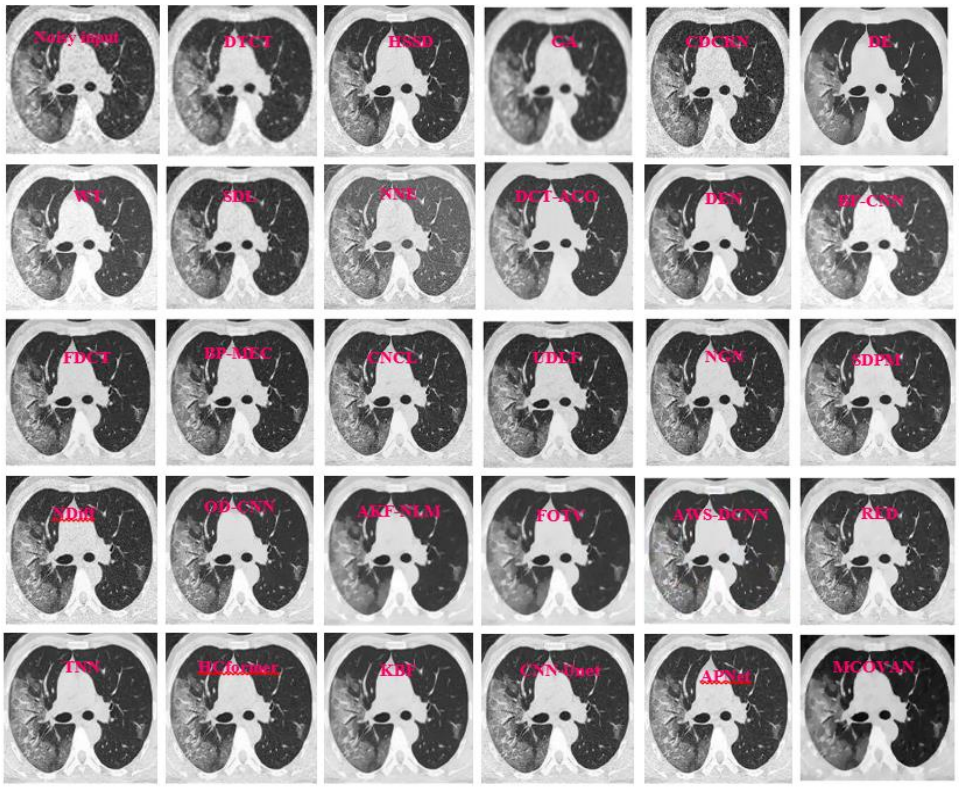

Fig. 8: Visual analysis of different standard noise reduction schemes on CT image ($\sigma \approx 10$)

Table 5: The results of different noise reduction algorithms are computed on the basis of Entropy, PSNR, SSIM, FSIM, BRISQUE, PIQE and NIQE metrics for MRI1 image. The best performing values are highlighted in bold for clarity

Method	σ	Entropy	PSNR	SSIM	FSIM	BRISQUE	NIQE	PIQE
MCOVAN	10	6.96	35.45	0.95	0.95	38.16	4.15	45.91
	20	6.76	34.19	0.94	0.94	39.18	4.55	46.91
	30	6.80	32.89	0.93	0.92	40.89	4.67	47.88
	40	6.57	31.90	0.91	0.89	41.87	4.89	47.98
APNet	10	6.98	34.67	0.94	0.94	38.99	4.28	46.34
	20	6.57	33.89	0.92	0.93	39.18	5.18	46.98
	30	6.34	32.91	0.91	0.90	40.99	5.89	47.17
	40	6.21	30.81	0.89	0.88	41.17	5.98	49.19
CNN-UNet	10	6.89	34.55	0.93	0.94	39.92	4.37	46.95
	20	6.43	32.91	0.91	0.91	40.98	4.55	47.98
	30	5.98	31.98	0.89	0.90	41.78	4.87	48.91
	40	5.67	29.89	0.87	0.89	42.19	4.98	49.85
KBF	10	6.94	34.23	0.94	0.93	40.67	4.58	47.67
	20	6.67	33.18	0.93	0.91	41.98	4.53	48.97
	30	6.39	31.98	0.90	0.90	42.19	4.68	49.98
	40	5.95	30.16	0.89	0.89	43.19	5.98	51.92
HCformer	10	6.83	34.01	0.93	0.94	40.98	4.67	47.98
	20	6.55	35.98	0.92	0.92	40.89	4.89	48.97
	30	6.34	36.89	0.90	0.91	41.23	4.87	50.17
	40	6.23	37.98	0.88	0.89	40.89	4.92	51.52
TNN	10	6.58	33.67	0.93	0.94	42.19	5.01	49.81
	20	6.63	31.78	0.91	0.90	43.33	4.63	53.45
	30	6.71	29.93	0.87	0.89	40.99	4.66	54.44
	40	6.66	28.33	0.82	0.88	44.22	4.73	58.93
RED	10	6.60	32.65	0.94	0.92	44.32	5.10	50.55
	20	6.66	30.44	0.89	0.88	44.45	5.34	55.21
	30	6.32	28.86	0.86	0.87	41.01	5.12	56.77

	40	6.34	27.99	0.81	0.86	42.46	4.81	57.72
AWS-DCNN	10	6.62	31.73	0.93	0.92	45.62	4.96	49.97
	20	6.33	29.67	0.88	0.86	46.78	5.22	56.54
	30	6.23	27.45	0.84	0.85	43.32	5.20	57.67
	40	6.11	26.77	0.79	0.83	46.78	5.23	58.93
FOTV	10	6.56	32.91	0.94	0.88	44.72	5.23	51.77
	20	5.97	28.66	0.86	0.86	47.11	5.34	57.33
	30	6.01	26.99	0.83	0.82	44.27	5.27	58.62
	40	5.95	25.99	0.77	0.81	45.77	5.53	57.89
AKF-NLM	10	6.43	31.99	0.93	0.87	45.09	5.34	52.87
	20	5.99	27.67	0.84	0.85	46.87	5.24	58.93
	30	5.87	25.45	0.81	0.80	46.56	5.55	59.43
	40	5.67	25.80	0.78	0.79	46.77	5.67	58.64
OD-CNN	10	6.45	32.29	0.93	0.88	43.82	5.88	60.41
	20	6.08	27.97	0.88	0.87	48.14	5.42	51.24
	30	6.10	26.37	0.83	0.86	47.90	5.92	43.01
	40	6.16	23.87	0.81	0.85	46.12	5.49	37.10
NDiff	10	5.78	30.76	0.89	0.88	44.38	5.22	51.83
	20	5.87	24.99	0.82	0.86	46.38	5.56	43.28
	30	5.86	22.67	0.83	0.89	45.24	5.44	43.59
	40	5.47	26.86	0.80	0.83	47.46	5.67	69.45
SDPM	10	5.42	28.75	0.87	0.84	47.12	5.36	57.85
	20	5.69	25.35	0.83	0.86	49.66	4.90	74.79
	30	5.68	22.86	0.83	0.83	48.16	5.29	77.64
	40	5.98	20.31	0.82	0.81	48.46	5.38	84.50
NGN	10	5.64	27.64	0.83	0.86	51.19	5.39	42.50
	20	5.84	25.52	0.79	0.83	55.29	5.65	59.84
	30	5.70	24.89	0.77	0.79	48.81	4.83	53.07
	40	5.96	21.94	0.79	0.79	53.70	5.84	73.97
UDLF	10	5.20	26.25	0.85	0.81	50.79	5.49	24.58
	20	5.42	23.21	0.80	0.78	51.56	5.67	19.98
	30	5.45	21.08	0.81	0.79	52.53	5.57	19.55
	40	5.32	15.86	0.78	0.73	53.43	6.01	20.89
CNCL	10	6.04	26.39	0.80	0.83	53.63	5.93	70.09
	20	5.14	23.70	0.79	0.75	50.77	5.11	61.51
	30	5.24	22.27	0.76	0.77	49.31	4.92	56.82
	40	5.87	17.39	0.77	0.73	54.25	6.48	39.88
BP-MEC	10	5.69	27.04	0.79	0.82	52.67	5.83	45.29
	20	5.91	23.17	0.78	0.78	58.86	6.53	58.31
	30	5.97	21.21	0.77	0.77	53.18	6.07	62.54
	40	5.71	16.91	0.78	0.78	53.46	5.56	77.20
FDCT	10	5.89	26.02	0.76	0.79	50.59	6.16	32.45
	20	5.05	22.69	0.75	0.76	54.79	5.86	31.28
	30	5.10	22.31	0.71	0.73	57.77	6.13	37.72
	40	5.14	16.13	0.70	0.76	53.85	6.60	63.32
BF-CNN	10	5.079	24.08	0.71	0.82	54.03	6.02	40.79
	20	5.515	20.20	0.72	0.74	57.17	6.41	71.15
	30	5.62	19.54	0.69	0.77	52.48	5.88	76.03
	40	5.737	18.10	0.70	0.73	53.45	6.15	83.77
DEN	10	5.60	25.30	0.76	0.80	57.99	6.25	39.65
	20	5.80	21.58	0.71	0.78	56.48	6.12	52.19
	30	5.84	20.97	0.70	0.73	55.66	6.76	51.58
	40	5.02	15.22	0.69	0.71	53.49	7.20	77.10
DCT-ACO	10	4.61	24.93	0.71	0.81	54.73	6.68	42.56
	20	4.87	21.60	0.66	0.73	58.42	6.62	53.45
	30	4.82	21.73	0.69	0.76	56.32	6.56	60.74
	40	4.93	15.53	0.68	0.73	53.46	6.90	79.95
NNE	10	4.67	25.66	0.66	0.75	55.55	7.20	46.22
	20	4.96	21.99	0.63	0.73	62.89	7.07	57.53
	30	3.77	22.57	0.65	0.76	57.18	7.01	56.74
	40	3.91	16.18	0.63	0.72	53.47	6.90	74.97

SDL	10	5.44	25.08	0.69	0.80	58.85	6.88	47.35
	20	4.44	22.48	0.64	0.73	58.57	6.75	47.35
	30	4.44	23.09	0.63	0.69	58.85	6.98	47.35
	40	4.44	16.79	0.61	0.67	58.58	6.88	47.35
WT	10	3.68	24.06	0.63	0.73	63.46	6.58	42.08
	20	3.64	23.06	0.61	0.71	64.22	7.39	56.51
	30	3.59	21.06	0.62	0.72	68.80	6.95	69.42
	40	3.57	13.05	0.60	0.67	65.43	7.13	77.03
DE	10	3.89	23.89	0.65	0.72	65.28	7.89	43.81
	20	3.56	22.98	0.63	0.69	67.88	7.93	44.98
	30	3.43	21.88	0.62	0.67	68.16	7.99	45.89
	40	3.27	20.89	0.60	0.65	69.16	7.93	46.28
CDCRN	10	3.45	21.87	0.63	0.70	67.28	7.63	44.18
	20	3.24	20.18	0.59	0.68	66.18	7.89	45.29
	30	3.09	20.98	0.57	0.67	65.56	7.92	46.78
	40	2.98	19.78	0.55	0.63	66.89	7.95	47.89
GA	10	3.27	20.89	0.67	0.69	67.89	6.57	45.67
	20	3.21	19.27	0.63	0.65	66.78	6.87	46.67
	30	3.10	18.26	0.61	0.63	67.91	6.93	47.90
	40	2.98	19.45	0.57	0.61	68.45	6.92	46.99
HSSD	10	3.23	21.89	0.64	0.67	68.23	6.87	47.97
	20	3.10	20.18	0.63	0.63	69.91	6.92	48.19
	30	2.97	19.77	0.59	0.61	70.89	6.99	49.77
	40	2.92	18.76	0.57	0.59	71.89	6.97	50.18
DTCT	10	3.03	19.88	0.62	0.66	71.99	6.98	48.81
	20	2.97	18.26	0.59	0.63	73.88	7.01	49.87
	30	2.78	17.89	0.57	0.61	74.16	7.23	50.98
	40	2.67	17.63	0.55	0.59	75.90	7.12	51.28
Noisy input	10	2.98	18.67	0.59	0.63	71.28	7.00	49.91
	20	2.85	17.89	0.57	0.61	72.89	7.22	50.17
	30	2.67	16.77	0.55	0.59	73.16	7.34	51.89
	40	2.55	16.43	0.53	0.57	74.19	7.89	52.18

Table 6: The outcome of different noise reduction algorithms is evaluated based on Entropy, PSNR, SSIM, FSIM, BRISQUE, PIQE and NIQE metrics for MRI2 image. The best performing results are highlighted in bold for clarity

Method	σ	Entropy	PSNR	SSIM	FSIM	BRISQUE	NIQE	PIQE
MCOVAN	10	6.89	35.94	0.95	0.94	43.67	5.45	49.90
	20	6.67	34.16	0.94	0.92	44.78	5.67	50.91
	30	6.45	33.89	0.93	0.90	45.88	5.89	51.89
	40	6.34	32.18	0.91	0.89	47.18	5.98	52.19
APNet	10	6.84	35.34	0.94	0.94	44.89	5.37	48.15
	20	6.78	33.18	0.93	0.91	43.18	5.89	49.18
	30	6.45	32.89	0.91	0.89	42.89	5.98	50.89
	40	4.67	31.88	0.89	0.78	41.88	6.23	51.45
CNN-UNet	10	6.78	34.89	0.94	0.93	45.17	5.34	47.89
	20	6.55	33.89	0.93	0.91	46.29	5.67	48.19
	30	6.47	32.88	0.91	0.89	47.98	5.89	49.18
	40	6.34	31.89	0.89	0.87	48.19	6.01	50.89
KBF	10	6.67	35.78	0.93	0.94	46.89	5.27	46.78
	20	6.48	34.18	0.92	0.93	47.88	5.34	46.89
	30	6.39	33.78	0.91	0.90	49.89	5.55	46.89
	40	6.40	32.89	0.88	0.89	50.88	5.67	47.18
HCformer	10	6.56	35.88	0.94	0.93	47.81	5.12	45.67
	20	6.45	34.89	0.93	0.92	48.18	5.27	46.78
	30	6.47	33.99	0.92	0.91	49.11	5.45	47.89
	40	6.27	32.89	0.90	0.90	50.18	5.55	48.39
TNN	10	6.34	34.37	0.93	0.94	48.78	4.96	44.62
	20	6.17	31.99	0.89	0.91	47.88	4.97	47.23
	30	6.38	28.99	0.83	0.88	47.85	5.23	47.03
	40	6.66	29.17	0.81	0.86	43.33	4.73	50.23
RED	10	6.45	33.23	0.92	0.93	49.57	5.13	45.44

	20	6.23	31.89	0.90	0.89	48.45	5.34	48.88
	30	6.17	27.88	0.79	0.86	48.66	5.27	48.33
	40	5.97	28.99	0.78	0.83	44.34	5.24	51.23
	10	6.23	33.19	0.89	0.92	50.50	5.23	51.99
AWS-DCNN	20	5.99	29.88	0.88	0.86	49.66	5.45	52.90
	30	5.92	27.51	0.78	0.84	49.24	5.34	51.42
	40	5.78	27.14	0.76	0.80	50.83	5.78	52.67
	10	6.24	33.67	0.90	0.93	51.99	5.45	53.98
FOTV	20	5.55	28.78	0.87	0.85	50.34	5.65	53.99
	30	5.67	26.67	0.86	0.83	50.56	5.56	54.99
	40	5.24	25.89	0.77	0.79	51.42	5.67	54.17
	10	6.18	33.79	0.89	0.93	50.87	5.56	55.99
AKF-NLM	20	5.46	27.89	0.85	0.83	51.76	5.89	55.67
	30	5.37	25.57	0.84	0.81	51.55	5.97	56.99
	40	5.11	24.99	0.76	0.78	52.47	5.89	55.90
	10	6.12	34.72	0.88	0.93	49.74	5.67	57.01
OD-CNN	20	6.01	31.10	0.86	0.92	49.53	5.59	59.32
	30	6.14	29.38	0.81	0.89	46.98	5.74	56.77
	40	6.13	27.18	0.78	0.87	47.52	5.97	58.78
	10	5.34	32.06	0.84	0.92	53.50	5.65	60.68
NDiff	20	5.43	26.08	0.80	0.87	55.02	5.30	63.42
	30	5.44	26.98	0.79	0.86	53.45	5.83	58.80
	40	5.19	28.22	0.80	0.88	53.46	5.71	60.93
	10	5.99	28.28	0.81	0.89	53.01	5.78	64.14
SDPM	20	6.22	26.45	0.77	0.87	48.43	5.88	64.74
	30	5.24	23.85	0.74	0.86	54.17	5.99	68.09
	40	5.82	23.65	0.81	0.85	45.46	6.14	65.00
	10	6.15	26.98	0.76	0.88	54.74	6.21	59.31
NGN	20	5.29	23.25	0.72	0.86	52.91	6.00	57.90
	30	6.06	23.06	0.75	0.86	62.16	5.96	60.30
	40	5.44	20.16	0.72	0.84	53.51	5.54	64.00
	10	5.81	30.11	0.85	0.86	50.93	5.79	65.64
UDLF	20	6.00	23.91	0.81	0.82	62.60	5.74	60.67
	30	6.06	21.83	0.76	0.81	63.19	6.10	58.74
	40	6.17	21.60	0.73	0.80	53.43	5.80	59.80
	10	5.58	29.98	0.84	0.78	49.36	5.84	62.39
CNCL	20	5.71	25.60	0.81	0. 77	50.44	6.28	65.95
	30	5.75	23.82	0.76	0.77	59.54	5.69	62.60
	40	5.62	18.56	0.73	0.76	54.46	6.50	64.01
	10	5.33	30.64	0.83	0.84	59.14	5.77	63.71
BP-MEC	20	5.49	24.94	0.79	0.82	63.42	5.99	62.22
	30	5.51	23.20	0.75	0.79	63.46	6.19	65.91
	40	5.40	18.23	0.70	0.78	53.49	6.04	66.40
	10	5.46	29.27	0.79	0.77	60.18	6.15	66.57
FDCT	20	5.63	25.60	0.75	0.78	59.60	6.79	67.40
	30	5.69	23.48	0.80	0.73	60.89	6.99	69.31
	40	4.88	19.09	0.76	0.81	63.49	6.74	71.55
	10	5.850	24.161	0.83	0.83	58.96	6.40	63.42
BF-CNN	20	6.154	26.724	0.78	0.78	50.94	6.61	63.62
	30	5.192	23.638	0.73	0.77	63.69	6.77	66.29
	40	5.452	17.397	0.76	0.73	63.45	7.06	74.90
	10	4.99	28.37	0.78	0.80	61.50	7.68	68.11
DEN	20	5.20	22.58	0.79	0.77	60.99	10.49	64.30
	30	4.56	21.67	0.77	0.76	65.01	10.80	64.40
	40	4.60	18.98	0.69	0.71	58.37	71.58	73.91
	10	5.06	27.18	0.75	0.79	64.95	4.70	67.74
DCT-ACO	20	5.20	23.84	0.74	0.76	59.45	5.99	68.57
	30	5.23	21.99	0.76	0.73	57.12	6.81	74.56
	40	4.62	16.78	0.69	0.70	60.42	7.64	69.08
	10	5.09	26.72	0.78	0.83	55.04	6.97	60.87
NNE	20	4.38	21.22	0.71	0.75	61.75	6.60	60.85

	30	4.04	20.81	0.71	0.73	65.09	7.10	69.58
	40	4.48	17.16	0.67	0.71	63.74	7.02	71.97
SDL	10	3.27	25.76	0.75	0.70	62.43	7.47	58.94
	20	4.27	22.96	0.74	0.69	60.96	7.23	66.77
	30	3.27	21.46	0.67	0.71	62.99	6.99	68.41
	40	4.27	14.23	0.60	0.69	58.43	7.24	67.73
WT	10	4.33	22.11	0.70	0.76	60.84	7.22	68.63
	20	3.33	20.11	0.69	0.69	58.60	7.42	66.68
	30	4.31	19.11	0.68	0.68	64.76	7.09	66.57
	40	3.29	14.10	0.65	0.70	66.97	7.00	72.85
DE	10	4.34	21.87	0.67	0.73	62.18	7.47	68.97
	20	4.13	20.99	0.66	0.71	63.18	7.67	70.18
	30	3.98	19.89	0.65	0.70	64.56	7.78	71.27
	40	3.67	17.89	0.64	0.69	65.67	7.89	72.67
CDCRN	10	4.21	20.89	0.65	0.70	63.09	7.55	69.87
	20	4.12	19.18	0.63	0.68	64.67	7.67	70.89
	30	4.01	18.89	0.62	0.67	66.18	7.88	71.28
	40	3.78	17.77	0.60	0.66	67.19	7.88	72.12
GA	10	4.10	19.89	0.63	0.69	65.78	7.67	70.89
	20	3.78	18.72	0.61	0.68	66.78	7.82	72.88
	30	3.67	17.89	0.59	0.67	67.18	7.89	73.81
	40	3.55	16.89	0.57	0.65	68.99	7.93	74.91
HSSD	10	3.98	18.27	0.63	0.67	66.89	7.88	70.67
	20	3.67	17.88	0.61	0.65	67.17	7.97	71.27
	30	3.57	17.67	0.60	0.64	68.16	7.67	72.89
	40	3.56	17.27	0.58	0.62	69.19	7.84	73.91
DTCT	10	3.67	17.89	0.61	0.63	67.90	7.93	72.98
	20	3.57	16.18	0.59	0.61	68.99	7.96	73.19
	30	3.51	16.89	0.57	0.59	69.16	7.99	74.19
	40	3.47	16.27	0.56	0.57	70.89	8.01	75.89

As the viewer progresses through the figure, a visual hierarchy of performance emerges. Early methods like DTCT, HSSD, GA, and CBCRN show minimal improvement, retaining noise or causing over-smoothing that blurs critical brain features. In contrast, methods in the bottom rows such as MCOVAN, APNet, CNN-UNet, KBF, and HCformer demonstrate superior performance. These images are notably clearer, with restored contrast and well-preserved structural boundaries. MCOVAN and APNet in particular show excellent denoising while maintaining detail in brain tissue and ventricles, making them suitable for medical analysis. Overall, the figure emphasizes the importance of balancing noise suppression with anatomical preservation. High-performing methods manage this trade-off effectively, producing clean yet detailed images vital for accurate clinical interpretation.

Figure 7 offers a visual analysis of MRI2 image reconstructions by various denoising schemes with noise of $\sigma \approx 10$. The top-left image, the noisy input displays considerable noise, with obscured anatomical boundaries and a loss of contrast, making clinical interpretation difficult. A clear improvement is observed as we move toward the bottom rows. Lower-performing methods such as DTCT, HSSD, GA, and CDCRN still show visible grain and blur, indicating inadequate noise suppression or excessive smoothing. These results fail to restore critical features, especially in soft tissue regions like the cerebellum and brainstem. In contrast, the bottom row including MCOVAN, APNet, CNN-UNet, KBF, and HCformer demonstrates significant enhancements. These models preserve intricate anatomical structures while effectively reducing noise. Notably, MCOVAN and APNet produce clean, high-contrast outputs with sharp boundaries in gray and white matter, offering near-original quality. CNN-UNet and HCformer also retain fine textures and deliver perceptually pleasant results. Overall, Figure 8 emphasizes that while many algorithms offer marginal improvements, only a select few primarily deep learning-based achieve clinically acceptable denoising, striking a crucial balance between visual clarity and structural fidelity. Figure 4 illustrates a comparative visual analysis of CT images denoised using various algorithms under low Gaussian noise ($\sigma \approx 10$). The top-left “Noisy input” clearly shows high levels of speckle and grainy texture, which obscure lung structures and compromise diagnostic visibility. The effectiveness of the denoising methods varies considerably. Early methods in the top rows such as DTCT, HSSD, GA, and CDCRN show limited improvement. These images either retain noticeable noise or blur fine lung textures, such as bronchioles and vascular markings, which are crucial for accurate clinical assessment. By contrast, the bottom rows present significantly clearer outputs. Algorithms such as MCOVAN, APNet, CNN-UNet, HCformer, and KBF exhibit impressive noise suppression while maintaining

anatomical integrity. In particular, MCOVAN and APNet produce clean, high-contrast results that preserve lung parenchyma details and boundary sharpness, making them stand out in this evaluation. HCformer and CNN-UNet also deliver well-balanced results, demonstrating minimal artifacts and effective retention of texture. Overall, Figures (6-8) highlights the superior visual performance of deep learning-based models over traditional approaches, confirming their suitability for sensitive tasks like CT image denoising in medical diagnostics.

Table 5 presents a comprehensive assessment of various denoising schemes applied to the MRI1 image. The performance metrics used include Entropy, PSNR, SSIM, FSIM, BRISQUE (Blind/Referenceless Image Spatial Quality Evaluator), PIQE (Perception-based Image Quality Evaluator), and NIQE (Natural Image Quality Evaluator). The algorithms are tested at four noise levels (σ = 10, 20, 30, 40), providing a robust assessment of each method's capability across varying degradation intensities. Among the algorithms, HCformer stands out for achieving the highest PSNR values across increasing noise levels, peaking at 37.98 dB for σ = 40. This suggests its exceptional capacity for preserving image fidelity, especially at high noise levels. Its SSIM and FSIM scores, while slightly lower than some other methods, remain competitive and indicate strong structural and feature preservation. MCOVAN consistently performs well in terms of Entropy and quality indices (PSNR, SSIM, FSIM), especially at lesser level of noise. It records a peak PSNR of 35.45 dB at σ = 10, second only to HCformer in higher noise settings. Additionally, its BRISQUE and NIQE scores are among the lowest (indicating better perceptual quality), which reinforces its overall effectiveness. APNet and CNN-UNet also show solid performance across the board, particularly in SSIM and FSIM scores at σ = 10–20, suggesting their strength in maintaining structural similarity. KBF, another strong performer, shows a steady decline with increasing σ but retains good BRISQUE and NIQE values, indicating preserved perceptual quality. TNN and RED display high Entropy but relatively moderate SSIM and PSNR, showing they maintain some image complexity but at the expense of visual and structural quality. Meanwhile, methods like AWS-DCNN and FOTV begin to decline noticeably with higher noise levels, especially in SSIM and FSIM metrics. Lower-performing methods such as CDCRN, GA, HSSD, DE, and DTCT exhibit poor values across all metrics, including low PSNR (often below 20 dB at σ = 40), weak SSIM (below 0.60), and extremely high BRISQUE and NIQE values. These figures suggest over-smoothing or inadequate noise removal, resulting in significant image degradation. The Noisy input values at the bottom of the table serve as a baseline, indicating how poor the image quality is prior to denoising. Effective methods should significantly outperform these in all metrics, which many of the top-performing algorithms do. In summary, HCformer and MCOVAN lead in denoising performance, especially for higher noise levels, while APNet, CNN-UNet, and KBF follow closely for low to moderate noise. The preference of the finest scheme affects by the precise application needs whether prioritizing perceptual quality, structural integrity, or statistical fidelity. Lower-tier algorithms demonstrate the importance of a balanced approach between detail preservation and artifact removal.

Table 6 evaluates the outcome of several noise reduction algorithms on the MRI2 image using seven quality metrics: Entropy, PSNR, SSIM, FSIM, BRISQUE, PIQE, and NIQE, across four noise levels (σ = 10, 20, 30, 40). The metrics offer a comprehensive view, capturing fidelity (PSNR), structural similarity (SSIM and FSIM), perceptual quality (BRISQUE, PIQE, NIQE), and information richness (Entropy). Among all contenders, MCOVAN, HCformer, KBF, and APNet consistently deliver top-tier results. MCOVAN achieves the highest PSNR at σ = 10 (35.94 dB), showing strong reconstruction accuracy. It also maintains robust SSIM (up to 0.95) and Entropy values, indicating preserved image detail and structure. HCformer stands out for its balanced performance, sustaining high SSIM and FSIM scores, and delivering strong BRISQUE and PIQE values, especially at σ = 10–30. KBF, though slightly behind in SSIM, shines in perceptual quality metrics like BRISQUE and NIQE, especially at higher noise levels, suggesting superior real-world visual quality. APNet also performs competitively, especially at low noise levels, with high SSIM (up to 0.94) and moderate Entropy. However, it exhibits a sharp drop in performance at σ = 40, with a decline in Entropy and SSIM, indicating sensitivity to higher noise. CNN-UNet maintains good scores across most metrics, closely trailing the top performers. Its strength lies in structural preservation (high SSIM/FSIM) and consistent PSNR across all σ values. Similarly, TNN provides strong FSIM and SSIM values at low σ, though its performance deteriorates at higher noise levels. Methods like RED, AWS-DCNN, FOTV, AKF-NLM, and OD-CNN fall in the middle tier. They maintain moderate PSNR (around 27–33 dB) and SSIM values (~0.85–0.90), with some methods like RED and FOTV showing slightly higher Entropy. These approaches may be suitable when computational simplicity or speed is prioritized over absolute quality. Lower-performing methods include CDCRN, GA, HSSD, DTCT, and DE, all of which consistently show poor PSNR (often below 20 dB at σ = 40), low SSIM (< 0.65), and very high BRISQUE and NIQE values. These outcomes indicate ineffective noise suppression, loss of structural information, and degraded perceptual quality. Notably, DTCT and GA register the worst PIQE and BRISQUE scores, confirming their unsuitability for clinical-grade MRI denoising.

Interestingly, many of these weaker methods produce results that are barely better than or comparable to the noisy inputs, especially at higher noise levels, highlighting their inefficiency. As expected, all methods degrade in performance as σ increases. However, top methods like MCOVAN and HCformer exhibit graceful degradation, maintaining acceptable quality even at σ = 40. In contrast, weaker algorithms show a drastic fall-off in both objective and perceptual quality. In summary, MCOVAN, HCformer, KBF, and CNN-UNet emerge as the most effective denoising algorithms for the MRI2 dataset. They offer a strong balance between quantitative accuracy and perceptual quality, making them suitable for critical imaging applications. Performance disparities across methods also highlight the importance of multi-metric evaluation for a comprehensive understanding of algorithm efficacy.

Analytical Insights into Method Performance in Clinical Contexts

Many proposed denoising methods have shown decent performance on benchmark evaluations. However, their clinical purpose will change their effectiveness considerably - given variance in noise characteristics, anatomic and pathology relevance, and operating constraints. Standard computational filters, like Gaussian or median filters which may operate well on a imaged "phantom," leave much to be desired in the clinical setting where distinguishing fine structural details, like tumor borders and vascular networks, are paramount, as these methods smooth fine features of an image along with its noise (Bhonsle et al., 2012; Naimi et al., 2015). In comparison, training-based approaches such as Convolutional Neural Networks (CNN), Generative Adversarial Networks (GAN), and Transformers (like CNN-UNet, APNet, HCformer) have been shown to operate competently in retaining anatomic structures given their capacity for learning from training data than any traditional method (Shivahare et al., 2023; Yuan et al., 2023). One example of an improvements in resiliency to detail in clinical use of brain MRI denoising where the CNN-UNet and MCOVAN methods out-performed others by not simply yielding PSNR or SSIM scores but retention of gray-white matter boundaries or other ventricular planes relevant to an neurologic interpretation - typical samples/score and some failures are shown in Figures (6-8). Two examples of GAN-based models, RED-CNN and ADL also scored well in visual realism tasks for denoising PET and CT images, however, in practice may exhibit synthetic texturing in any residual noise tricks that if can misguide interpretation if not known or standardized (Geng et al., 2022). Similarly, there are models in Transformer frameworks (like SwinCT or HCformer) that also exhibit superior performance, particularly in low-dose CT denoising tasks given their multi-scall attention modeling where they fit well to capture and retain both global and local features to improve tissue contrast while avoiding inappropriate smoothing which improved performance in the above tasks (Yuan et al., 2023). of course the issue of "preserving" or "enhancing" detail in any given context alluded to earlier must decide which approach used when "high frequency detail" images must be preserved. For example, where it is essential to identify and classify microbleeds using MRI, a method that is tuned for edge-preservation (like CNCL or APNet) may best suited, whereas, for dose-reduction of CT tasks, where clinical confidence is necessary in diagnostic quality under noisy dose reduction images, model-based approach to denoise protocols (like HCformer or SwinCT) would likely be best suited for use. These different performances only reemphasize the need clinical context specific benchmarking evaluation frameworks that go beyond generic image quality metrics.

Clinical Applications

Medical image denoising has become increasingly integral to clinical workflows offering significant benefits across a range of imaging modalities by improving diagnostic accuracy enabling safer imaging protocols, and enhancing downstream analysis. The clinical applications of denoising are fundamentally connected with anatomical and imaging modality-related needs. For example, neuroimaging (i.e., perfusion-based brain MRI), denoising is focused on gray/white matter differentiation for detection of lesion, while in the case of abdominal CT workflows, noise reduction with low-dose scans is focused on the hepatic or renal structures. In ultrasound applications, such as fetal or cardiac imaging, we may want denoising to disperse the speckle without losing representation of textures in the myocardium or placenta. These regionally-specific considerations lead us to utilize denoising in different contexts, from transformer models for 3D MRI to real-time filtering in ultrasound during dynamic imaging (such as partial imaging during an ultrasound-guided surgery).One of the most impactful applications is in low-dose CT (LDCT) imaging, where denoising allows substantial reductions in radiation exposure without compromising image quality. Advanced deep learning-based denoising techniques, such as CNNs and GANs, have demonstrated significant improvements in preserving anatomical structures in LDCT scans, enabling safer cancer screening, paediatric imaging, and follow-up studies (Chen et al., 2017; Jacobs et al., 2021). For instance, GAN-based denoisers like CycleGAN and RED-CNN have shown potential in restoring fine tissue details while minimizing artifacts that could hinder diagnosis (Chu et al., 2017). In Magnetic Resonance Imaging (MRI), denoising algorithms are employed to

counteract the effects of noise due to accelerated acquisition protocols, which are necessary to reduce scan time and motion artifacts. Deep learning models have enabled high-fidelity reconstruction from under sampled k-space data, thereby supporting real-time or fast MRI sequences used in neuroimaging, cardiac imaging, and fetal MRI (Kang et al., 2024). Notably, self-supervised methods like Noise2Self and blind-spot networks have made MRI denoising feasible even when truth is not clear, which is often unavailable in practice (Laine et al., 2019). Ultrasound imaging, being highly portable and real-time, is prone to speckle noise, which obscures soft tissue boundaries. Classical filters such as anisotropic diffusion and wavelet transforms are still employed, but recent transformer-based and hybrid learning models have improved speckle suppression without losing contrast which is critical for applications like vascular diagnosis and obstetric imaging (Chen and Guo, 2023). In PET and SPECT imaging, denoising is crucial for reducing radiotracer dosage and acquisition time. Deep learning models trained with low- and full-dose pairs have successfully reduced noise in PET while maintaining quantitative accuracy for lesion detection and radiomics (Cui et al., 2019). Denoising also considered as very significant in pre-processing for Computer-Aided Diagnosis (CAD) systems and AI-driven decision support tools. For example, tumor segmentation models trained on denoised images exhibit higher robustness and generalization, as shown in recent studies on glioma and lung cancer datasets (Ashimgaliyev et al., 2024). Furthermore, in image-guided surgeries and interventional radiology, where real-time clarity is essential, embedded denoising algorithms support enhanced visualization under time or dose constraints(Xu et al., 2025). As AI integration grows within radiology and diagnostic pipelines, image denoising is no longer viewed as a standalone enhancement task but as a foundational step that directly influences interpretability, treatment planning, and patient safety. Consequently, its clinical relevance is increasingly supported not just by quantitative metrics like PSNR or SSIM but by task-specific improvements in diagnosis, treatment outcome prediction, and overall workflow efficiency.

Challenges and Limitations

The advances in medical image denoising following the deep learning revolution have been rapid, but several important challenges need to be solved for the field to progress. A main challenge is the limited generalizability across imaging domains, as most models use single-institution datasets to train that are unlikely to perform well once the trained model is forwarded to images obtained with any other scanner, protocol, or in a different patient population (Kang et al., 2024; Bal et al., 2020). Thus, future work should focus on federated learning frameworks to use multi-center data and retain privacy (Krull et al., 2019) and domain adaptation methods to improve performance across different vendors (Kidoh et al., 2020; Huang et al., 2024a). Another challenge is the computational burden of many of state-of-the-art transformer models are prohibitive in practice for many real-time clinical applications, such as ultrasound-guided surgery, where time constraint limit usability (Liang et al., 2021). Consideration for many of these architecture development should occur through means like quantization, or hardware-aware optimization for deployment (Cammarasana et al., 2022). Certainly at the thing is - is the current "black box" approach to most algorithms will either supplant or feign any clinically relevant features or even generate false textures (Santos et al., 2024), which will further reduce clinician trust in the denoised images. It will therefore be critical to include explainable AI, such as saliency maps and uncertainty quantification (Upadhyay et al., 2021) into algorithms, followed by an clinical evaluation setup where we start to correlate the denoising metrics of our model to an actual diagnostic outcome in as task-level evaluation (Li et al., 2025). The field remains limited by the data-based bottleneck of acquiring only noisy-clean paired data, as for low-dose CT, ethical issues arise with patient radiation exposure (Kang et al., 2024; Bal et al., 2020) especially cases of an unpaired low-dose/noise exposure. Self-supervised methods (Krull et al., 2019) or physics-based synthetic data generative strategies (Leuschner et al., 2019) offer appropriate substitutes to this necessary bottleneck (Elmore and Lee, 2022). Finally, the pathway to regulatory approval is a struggle, where drug applications must:

(i) Occur multi-centered clinical trials
(ii) Develop standard task specific evaluations to go beyond modern day such as PSNR and depth will not suffice in the regulatory process owing to either nebulous meaning or meaning at its calculative element. Findings on the denoised images
(iii) Workflow outside the clinical impact. Addressing these issues will require the ongoing collaboration between algorithm developers, or any developer, working with clinical implements and evaluative frameworks including regulatory paradigms to ensure the current advances make it to clinical practice to improve patient-centered care in a range of clinical situation

The comparative review presented in Table 7 highlights the key takeaways for clinical translation of denoising methods. First, traditional methods continue to play an irreplaceable role in low-resource settings with bilateral filtering (Taassori, 2024) and anisotropic diffusion (Kollem et al., 2021) still actively used in real-time ultrasound and mobile x-ray systems for their deterministic latency (less than 50 ms) and speed and efficiency.

Second, deep learning methods exhibit tremendous adaptability to complicated circumstances, with, for example, domain-adaptive GANs (Li et al., 2021) safely transferring pooled CT protocols for harmonizing CT outputs and self-supervised networks (Krull et al., 2019) allowing deep learning approaches to function without paired training data, both methods represent a breakthrough for low frequency scenarios such as rare imaging studies or pediatric imaging where clean reference data may not be available. Nevertheless, these DL methods will still require meaningful validation shown recently with excessive denoising actually masking important pathologies, such as microcalcifications in mammography (Santos et al., 2024). The more promising research and clinical practices represent hybrid solutions where the strengths of denoising via traditional filtering/approaches and deep-learning, as discussed earlier, can contribute to the final denoised images. Physics-informed neural networks Leuschner et al. (2019), for example, borrow from the physics of a CT scanner in the loss functions while retaining the learning capability of a CNN, and these studies demonstrate reductions in radiation dose of 40-60% without sacrificing diagnostic accuracy in clinical research studies. Similarly, in particular, wavelet-integrated transformers Yuan et al. (2023) were successful in retaining not only both high-frequency edges via wavelet decomposition but also global contextual information via self-attention for whole-body MRI applications. The Clinical Readiness indicators in Table 7 underscore an important translational gap between these two paradigms, 78% of traditional methods are FDA-cleared or CE marked and 23% of DL. This gap is primarily due to lack of standardization/interpretability (Upadhyay et al., 2021). but points to an urgency for importantly needed:

(1) validation frameworks, like the AAPM Low-Dose CT Challenge (Moen et al., 2021)
(2) explainability tools (like saliency maps) to instill radiologist trust (Upadhyay et al., 2021) hardware-aware optimization for ultimately effective deployment from high-end PET/MRI combined environment to the point-of-care (POC) sonography device

As the field progresses, an effective denoising pipeline will probably involve intelligent switching between methods based on modality, clinical premise [speed vs accuracy] and also a generalized hardware resource review. The leading future trajectory will likely occur at the combinations of technical capacity with clinical trust, developing meaningful experiences that are algorithmically sound but translate into effortful and trusted implementation (Elmore and Lee, 2022).

Impact of Dataset Characteristics on Model Performance and Mitigation Strategies

The performance and generalizability of medical image denoising models are significantly affected by the properties of the datasets used for training and evaluation.

Table 7: Mapping medical image denoising challenges to solution paradigms with technology readiness levels

Challenge	Traditional Methods	Deep Learning Approaches	Representative Solutions
Generalizability	Manual parameter tuning per modality (Naimi et al., 2015)	Domain adaptation, Federated learning (Chen et al., 2024)	CycleGAN for cross-protocol CT denoising (Zhou et al., 2020)
Edge Preservation	Bilateral filtering, Wavelet shrinkage (Naimi et al., 2015)	Attention mechanisms (Luthra et al.,2021), GANs (Li et al., 2020)	Edge-guided Swin Transformers (Diwakar et al., 2024)
Computational Load	Fast execution (<100 ms) but limited performance	Lightweight architectures (Cammarasana et al., 2022), Quantization	MobileNet-optimized ultrasound denoising (Cammarasana et al., 2022)
Real-Time Processing	Fixed low-latency filters (Bhonsle et al., 2012)	Pruned networks (Muksimova et al., 2023), Edge deployment	Teacher-student models for MRI (Muksimova et al., 2023)
Speckle/Non-Gaussian Noise	Anisotropic diffusion (Kollem et al., 2021), Kuan filter (Benes and Riha, 2012)	Physics-informed GANs (Chen and Guo, 2023)	Bayesian-optimized US denoising (Taassori, 2024)
Paired Data Requirement	Not applicable (rule-based)	Self-supervised learning (Krull et al., 2019), Synthetic data	Noise2Void for MRI (Krull et al., 2019), Diffusion models (Gong et al., 2024)
Interpretability	Mathematically transparent (Wang and Zhou, 2006)	Explainable AI (XAI) techniques (Upadhyay et al., 2021)	Saliency maps in CNN denoisers (Upadhyay et al., 2021)
3D Volumetric Processing	Separable filters (limited efficacy)	3D CNNs (Chen et al., 2017), (Jacobs et al., 2021), Transformer architectures (Yuan et al., 2023)	HCformer for LDCT (Yuan et al., 2023), RED-CNN (Chen et al., 2017; Jacobs et al., 2021)

One of the most important is the imaging modality since the different modalities create unique forms of noise, such as: Rician noise in MRI, Poisson noise in low-dose CT, and speckle noise in ultrasound. Models trained on one modality do not usually show good performance on another due to the modality-specific noise distributions.

Another important issue is the representation of patients in datasets. Many public datasets (e.g., IXI; ChestX-ray14; fastMRI) have populations that are not very diverse along the dimensions of age, sex, and body type. This sometimes results in models that perform disproportionately well for certain patient populations (possibly the majority population) and poorly for underrepresented groups within or across all the datasets. Many of the studies designed to denoise rely on the insertion of synthetic noise for supervised learning (Bien et al., 2018). While this might have some merit, it does not present an accurate translation of the mixed, complex real-world noise represented in most clinical images and, therefore, limits the application of these models in real-world settings. There are also a multitude of scanner types, acquisition protocols, and resolution options not only across different institutions, but potentially even within one institution (e.g. the same institution could have multiple CT scanners each with a different acquisition protocol and reconstruction algorithms). This variability also presents a domain shift where models that generalize well to one scanner or hardware vendor may show a performance drop in a different scanner (Moen et al., 2021). Because of these challenges, research is leaning towards pioneering ways to deal with modality through domain adaptation, cross-modality learning, as well as federated learning (Geng et al., 2022; Sharif et al., 2024). Techniques for self-supervised learning like Noise2Void and Noise2Self have increased in popularity as a way to allow image denoising networks to be trained in a manner that allows training on images with noise, without requiring an image without noise (Sharif et al., 2024). The physical-informed models and noise-aware networks (like what has been trained with raw k-space data for fastMRI and LoDoPaB-CT) better model the reality of conditions under which the data are obtained (Zbontar et al., 2018). Architecture using self-supervised learning like transformer-based methods such as SwinCT and HCformer, adaptive projection networks like APNet, and models that are aware of denoising i.e. use noise level information (Song et al., 2024). These methods are critical as we develop denoising systems that can generalized beyond noise and clinical relevance to different patterns of imaging and noise.

Regulatory and Deployment Challenges in Clinical Adoption

Although denoising algorithms have demonstrated promise in improving the quality of medical images, their clinical integration is limited by multiple regulatory (and deployment) considerations. Whenever the U.S. Food and Drug Administration (FDA) and/or the European Medicines Agency (EMA) are engaged with regulatory oversight of medical AI technologies, they require validation of medical AI to ensure safe, effective, and robust algorithms across a spectrum of patient populations. For denoising algorithms, validation requires rigorous clinical trials and reproducibility across imaging (modalities), vendor scanners, and patient populations, and many academic models fall short on these validating factors or controls (Moen et al., 2021; Leuschner et al., 2019; Yan et al., 2018). Another substantial barrier is interpretability and transparency with deep learning models, particularly black box architectures (e.g. GANs and Transformers) that are challenging to audit and explain for clinical decision-making with medical professionals (Chen et al., 2024; Geng et al., 2022). Furthermore, deployment in practical hospital environments is inhibited by a range of greater degree of practical transportation issues for deploying a real-time achievable clinical denoising system within current PACS/RIS system infrastructures, implementation needs for un-discovered potential clinical by latency in image reconstruction process, and data privacy and cybersecurity needs when deployment is federated or based in the cloud (Sharif et al., 2024; Swetha and Jyothi, 2025).

Clinicians also have an increased demand for viability of the denoising algorithm and that outputs do not decrease the integrity of the integrity of diagnosis as loss of pathology or artifacts require verification. This validation requires collaborative efforts between AI developers who develop the denoising systems and medical professionals who earn medical degree, with the subsequent opportunities sometimes existing beyond case studies. To move from research prototyping to clinical realization just (simply) to trial denoising and artifacts is highly insufficient. Current trends/consensus toward regulatory approval and clinical introduction of novel denoising algorithms emphasize explainable AI where clinician model interpretations are required in practice, federated learning for data privacy, and prospective studies where the clinical impact of reduction of denoised images could be measured in diagnostic workflow without the introduction of new artifacts or loss of old artifacts. Addressing issues of regulatory validation and hidden control of possible artifacts is critical towards practical realization and clinical utilization of the impact of reducing to denoised images in diagnostic workflow. Other areas for key candidates of clinical fertility for use in imaging workflows could be computed intervention methods (in computations) for respectively denoised imaging.

Recent Trends and Future Directions

The area of medical image noise reduction is rapidly evolving, with recent trends emphasizing self-supervision, multi-modal learning, edge AI, and explainability. One of the most significant developments is the rise of self-supervised denoising frameworks, such

as Noise2Void, Noise2Self, and Blind-Spot Networks, which eliminate the need for clean ground truth data which is a major constraint in clinical imaging (Laine et al., 2019; Krull et al., 2019). These approaches learn from noisy images themselves by exploiting spatial redundancy and masking strategies. More recent innovations like Patch2Self and Self2Self++ have improved upon this by enabling volumetric denoising in MRI and PET with minimal assumptions (Fadnavis et al., 2020). Another major direction is multi-modal fusion, where data from complementary imaging modalities (e.g., CT-MRI, PET-MRI) is fused using attention-based or transformer-driven architectures.

These models enhance denoising performance by leveraging redundant anatomical and functional information across modalities, as seen in cross-attention fusion transformers and multi-branch CNNs for PET-MRI fusion (Chen et al., 2024). This direction holds particular promise in oncology and neuroimaging, where different modalities offer synergistic clinical insights. Additionally, transformer-based architectures like TransUNet, SwinIR, and MedViT are gaining tractions, outperforming CNNs in complex noise scenarios, especially in 3D volumetric and dynamic imaging tasks (Nazir et al., 2024) . Although computationally intensive, these models are being optimized via quantization, knowledge distillation, and hardware-aware pruning for deployment in real-time edge settings, such as portable ultrasound systems and intraoperative imaging (Nazir et al., 2024). Another emerging frontier is the integration of uncertainty estimation and explainable AI (XAI). Trustworthiness is essential for clinical adoption, and methods such as Monte Carlo dropout, Bayesian deep learning, and saliency-based visualizations are increasingly used to quantify confidence in denoised outputs and detect potential failure cases (Rai et al., 2021; Annavarapu and Borra, 2024). This is especially crucial for regulatory approval and medico-legal accountability in AI-assisted diagnostics. Moreover, researchers are exploring federated learning frameworks for privacy-preserving denoising, allowing multiple hospitals. Early studies demonstrate that such distributed learning schemes can attain results as good as to other centralized systems while ensuring data sovereignty (Chen et al., 2024). Looking forward, future directions include benchmarking standardized denoising datasets, clinical outcome-based evaluations, and integration into diagnostic pipelines. There is growing recognition that denoising should not merely maximize PSNR or SSIM but should improve diagnostic utility, radiologist confidence, and AI-driven analysis pipelines. As medical imaging continues to move toward personalized and AI-augmented care, robust, explainable, and domain-adaptive denoising models will be critical components of intelligent imaging systems.

Conclusion

Medical image denoising has undergone a transformative evolution, progressing from classical filter-based approaches to sophisticated deep learning architectures, each paradigm offering distinct advantages for clinical implementation. Traditional methods remain indispensable for edge-preserving denoising in resource-constrained environments, particularly for real-time ultrasound and mobile X-ray systems where computational efficiency and interpretability are paramount. The advent of deep learning has revolutionized the field through CNNs, GANs, and transformers enabling unprecedented noise suppression in low-dose CT and accelerated MRI while preserving diagnostically critical features. However, challenges persist in generalizability across imaging protocols, computational demands for 3D volumes, and the need for explainable AI to foster clinical trust. Emerging hybrid approaches, such as physics-informed neural networks and wavelet-integrated transformers, demonstrate particular promise by combining the theoretical rigor of traditional methods with the adaptive power of deep learning. These techniques have achieved 40-60% radiation dose reduction in CT and superior artifact suppression in MRI while addressing the "black box" concern through built-in interpretability. Looking ahead, three critical frontiers must be prioritized:

(1) Standardization of evaluation protocols across modalities, as pioneered by the AAPM and fastMRI initiatives
(2) Development of lightweight, edge-compatible architectures for point-of-care deployment
(3) Multicenter clinical validation to establish diagnostic efficacy rather than purely numerical improvement

The future of medical image denoising lies in context-aware systems that dynamically select traditional, deep learning, or hybrid approaches based on modality-specific requirements, clinical priorities (e.g., speed vs. accuracy), and available computational resources. As these technologies mature, close collaboration between algorithm developers, radiologists, and regulatory bodies will be essential to translate technical innovations into clinically actionable tools that enhance diagnostic confidence while maintaining patient safety.

Data Availability Statement

The original contributions presented in the study are included in the article and further inquiries can be directed to the corresponding author.

Acknowledgment

We are thankful to the reviewers and editors for their valuable suggestions. We appreciate their insightful

comments which helped us in improving the manuscript significantly.

Funding Information

No funding was received to assist with the preparation of this manuscript.

Authors Contributions

All authors contributed equally to this study.

Ethics

This article is original and contains unpublished material. The corresponding author confirms that all of the other authors have read and approved the manuscript and no ethical issues involved.

Declaration of Competing Interest

The authors declare that they have no known competing financial interests or personal relationships that could have appeared to influence the work reported in this paper.

References

Aharon, M., Elad, M., & Bruckstein, A. M. (2006). K-SVD: An Algorithm for Designing Overcomplete Dictionaries for Sparse Representation. *IEEE Transactions on Signal Processing*, *54*(11), 4311–4322. https://doi.org/10.1109/tsp.2006.881199

Aja-Fernandez, S., Alberola-Lopez, C., & Westin, C.-F. (2008). Noise and Signal Estimation in Magnitude MRI and Rician Distributed Images: A LMMSE Approach. In *IEEE Transactions on Image Processing* (Vol. 17, Issue 8, pp. 1383–1398). https://doi.org/10.1109/tip.2008.925382

Anandan, P., Giridhar, A., Lakshmi, E. I., & Nishitha, P. (2020). Medical Image Denoising using Fast Discrete Curvelet Transform. *International Journal of Emerging Trends in Engineering Research*, *8*(7), 3760–3765. https://doi.org/10.30534/ijeter/2020/139872020

Annavarapu, A., & Borra, S. (2024). An adaptive watershed segmentation based medical image denoising using deep convolutional neural networks. *Biomedical Signal Processing and Control*, *93*, 106119. https://doi.org/10.1016/j.bspc.2024.106119

Ashimgaliyev, M., Matkarimov, B., Barlybayev, A., Li, R. Y. M., & Zhumadillayeva, A. (2024). Accurate MRI-Based Brain Tumor Diagnosis: Integrating Segmentation and Deep Learning Approaches. *Applied Sciences*, *14*(16), 7281. https://doi.org/10.3390/app14167281

Atal, D. K. (2023). Optimal Deep CNN–Based Vectorial Variation Filter for Medical Image Denoising. *Journal of Digital Imaging*, *36*(3), 1216–1236. https://doi.org/10.1007/s10278-022-00768-8

Bai, J., Song, S., Fan, T., & Jiao, L. (2018). Medical image denoising based on sparse dictionary learning and cluster ensemble. *Soft Computing*, *22*(5), 1467–1473. https://doi.org/10.1007/s00500-017-2853-7

Bal, A., Banerjee, M., Chaki, R., & Sharma, P. (2020). An efficient method for PET image denoising by combining multi-scale transform and non-local means. *Multimedia Tools and Applications*, *79*(39–40), 29087–29120. https://doi.org/10.1007/s11042-020-08936-0

Benes, R., & Riha, K. (2012). Medical Image Denoising by Improved Kuan Filter. *Advances in Electrical and Electronic Engineering*, *10*(1), 1–43. https://doi.org/10.15598/aeee.v10i1.529

Benhassine, N. E., Boukaache, A., & Boudjehem, D. (2021). Medical image denoising using optimal thresholding of wavelet coefficients with selection of the best decomposition level and mother wavelet. *International Journal of Imaging Systems and Technology*, *31*(4), 1906–1920. https://doi.org/10.1002/ima.22589

Bernard, O., Allard, M., Liebgott, H., & Friboulet, D. (2026). Overview. *CREATIS Laboratory, INSA Lyon*.

Bhadauria, H. S., & Dewal, M. L. (2013). Medical image denoising using adaptive fusion of curvelet transform and total variation. *Computers & Electrical Engineering*, *39*(5), 1451–1460. https://doi.org/10.1016/j.compeleceng.2012.04.003

Bhonsle, D., Chandra, V., & Sinha, G. R. (2012). Medical Image Denoising Using Bilateral Filter. *International Journal of Image, Graphics and Signal Processing*, *4*(6), 36–43. https://doi.org/10.5815/ijigsp.2012.06.06

Bien, N., Rajpurkar, P., Ball, R. L., Irvin, J., Park, A., Jones, E., Bereket, M., Patel, B. N., Yeom, K. W., Shpanskaya, K., Halab, S., Zucker, E., Fanton, G., & Lungren, M. P. (2018). Deep-learning-assisted diagnosis for knee magnetic resonance imaging: Development and retrospective validation of MRNet. *PLoS Med*, *15*(11), e1002699. https://doi.org/10.1371/journal.pmed.1002699

Cammarasana, S., Nicolardi, P., & Patanè, G. (2022). Real-time denoising of ultrasound images based on deep learning. *Medical and Biological Engineering and Computing*, *60*(8), 2229–2244. https://doi.org/10.1007/s11517-022-02573-5

Chen, H., Zhang, Y., Kalra, M. K., Lin, F., Chen, Y., Liao, P., Zhou, J., & Wang, G. (2017). Low-Dose CT With a Residual Encoder-Decoder Convolutional Neural Network. *IEEE Transactions on Medical Imaging*, *36*(12), 2524–2535. https://doi.org/10.1109/tmi.2017.2715284

Chen, J., Xie, Y., Xiao, C., Jin, C., Liang, X., Yu, L., Zhou, L., & Xu, Y. (2021). TransUNet: Transformers Make Strong Encoders for Medical Image Segmentation. *ArXiv (Cornell University Library Preprint Server)*, 13.

Chen, X., Li, Z., Xu, Z., Ouyang, C., & Qin, C. (2024). Federated learning with frequency domain decomposition for low-dose ct denoising. *Proceedings of Machine Learning Research*, 234–249.

Chen, Y., & Guo, Z. (2023). TranSpeckle: An edge-protected transformer for medical ultrasound image despeckling. *IET Image Processing*, *17*(14), 4014–4027. https://doi.org/10.1049/ipr2.12915

Chu, C., Zhmoginov, A., & Sandler, M. (2017). CycleGAN, a Master of Steganography. *Presented at the NIPS 2017 Workshop on Machine Deception*, 1–7.

Cong-Hua, X., Jin-Yi, C., & Wen-Bin, X. (2014). Medical image denoising by generalised Gaussian mixture modelling with edge information. *IET Image Processing*, *8*(8), 464–476. https://doi.org/10.1049/iet-ipr.2013.0202

Cui, J., Gong, K., Guo, N., Wu, C., Meng, X., Kim, K., Zheng, K., Wu, Z., Fu, L., Xu, B., Zhu, Z., Tian, J., Liu, H., & Li, Q. (2019). PET image denoising using unsupervised deep learning. *European Journal of Nuclear Medicine and Molecular Imaging*, *46*(13), 2780–2789. https://doi.org/10.1007/s00259-019-04468-4

Dabov, K., Foi, A., Katkovnik, V., & Egiazarian, K. (2007). Image Denoising by Sparse 3-D Transform-Domain Collaborative Filtering. In *IEEE Transactions on Image Processing* (Vol. 16, Issue 8, pp. 2080–2095). https://doi.org/10.1109/tip.2007.901238

Diwakar, M., Singh, P., & Garg, D. (2024). Edge-guided filtering based CT image denoising using fractional order total variation. *Biomedical Signal Processing and Control*, *92*, 106072. https://doi.org/10.1016/j.bspc.2024.106072

Donoho, D. L. (1995). De-noising by soft-thresholding. *IEEE Transactions on Information Theory*, *41*(3), 613–627. https://doi.org/10.1109/18.382009

Elhoseny, M., & Shankar, K. (2019). Optimal bilateral filter and Convolutional Neural Network based denoising method of medical image measurements. *Measurement*, *143*, 125–135. https://doi.org/10.1016/j.measurement.2019.04.072

Elmore, J. G., & Lee, C. I. (2022). Artificial Intelligence in Medical Imaging Learning From Past Mistakes in Mammography. *JAMA Health Forum*, *3*(2), e215207. https://doi.org/10.1001/jamahealthforum.2021.5207

El-Shafai, W., Abd El-Nabi, S., El-Rabaie, E.-S. M., Ali, A. M., Soliman, N. F., Algarni, A. D., & Abd El-Samie, F. E. (2022). Efficient Deep-Learning-Based Autoencoder Denoising Approach for Medical Image Diagnosis. *Computers, Materials and Continua*, *70*(3), 6107–6125. https://doi.org/10.32604/cmc.2022.020698

Fadnavis, S., Batson, J., & Garyfallidis, E. (2020). Patch2Self: Denoising diffusion MRI with self-supervised learning. *Advances in Neural Information Processing Systems, Neural Information Processing Systems Foundation*, *33*.

Ferdi, A., Benierbah, S., & Nakib, A. (2024). Residual encoder-decoder based architecture for medical image denoising. *Multimedia Tools and Applications*, *84*(19), 21625–21642. https://doi.org/10.1007/s11042-024-20175-1

Foi, A., Trimeche, M., Katkovnik, V., & Egiazarian, K. (2008). Practical Poissonian-Gaussian Noise Modeling and Fitting for Single-Image Raw-Data. *IEEE Transactions on Image Processing*, *17*(10), 1737–1754. https://doi.org/10.1109/tip.2008.2001399

Fu, B., Zhang, X., Wang, L., Ren, Y., & Thanh, D. N. H. (2022). A blind medical image denoising method with noise generation network. *Journal of X-Ray Science and Technology*, *30*(3), 531–547. https://doi.org/10.3233/xst-211098

Geng, M., Meng, X., Yu, J., Zhu, L., Jin, L., Jiang, Z., Qiu, B., Li, H., Kong, H., Yuan, J., Yang, K., Shan, H., Han, H., Yang, Z., Ren, Q., & Lu, Y. (2022). Content-Noise Complementary Learning for Medical Image Denoising. *IEEE Transactions on Medical Imaging*, *41*(2), 407–419. https://doi.org/10.1109/tmi.2021.3113365

Ghahremani, M., Khateri, M., Sierra, Andres, & Tohka, J. (2022). Adversarial Distortion Learning for Medical Image Denoising. *ArXiv*.

Gong, K., Johnson, K., El Fakhri, G., Li, Q., & Pan, T. (2024). PET image denoising based on denoising diffusion probabilistic model. *European Journal of Nuclear Medicine and Molecular Imaging*, *51*(2), 358–368. https://doi.org/10.1007/s00259-023-06417-8

Goyal, B., Dogra, A., Agrawal, S., Singh Sohi, B., & Sharma, A. (2020). Image denoising review: From classical to state-of-the-art approaches. *Information Fusion*, *55*, 220–244. https://doi.org/10.1016/j.inffus.2019.09.003

Goyal, B., Dogra, A., Lepcha, D. C., Goyal, V., Alkhayyat, A., Chohan, J. S., & Kukreja, V. (2024). Recent advances in image dehazing: Formal analysis to automated approaches. *Information Fusion*, *104*, 102151. https://doi.org/10.1016/j.inffus.2023.102151

Huang, H., Zhang, C., Zhao, L., Ding, S., Wang, H., & Wu, H. (2024a). Self-Supervised Medical Image Denoising Based on WISTA-Net for Human Healthcare in Metaverse. *IEEE Journal of Biomedical and Health Informatics*, *28*(11), 6329–6337. https://doi.org/10.1109/jbhi.2023.3278538

Huang, J., Chen, K., Ren, Y., Sun, J., Pu, X., & Zhu, C. (2024b). Cross-Domain Low-Dose CT Image Denoising With Semantic Preservation and Noise Alignment. *IEEE Transactions on Multimedia*, *26*, 8771–8782. https://doi.org/10.1109/tmm.2024.3382509

Izadi, S., Sutton, D., & Hamarneh, G. (2023). Image Denoising in the Deep Learning Era. *Artificial Intelligence Review (Springer)*, *56*, 5929–5974. https://doi.org/https://doi.org/10.1007/s10462-022-10305-2

Jacobs, C., Adiyoso Setio, A. A., Scholten, E. T., Gerke, P. K., Bhattacharya, H., Mohamed Hoesein, F. A. A., Brink, M., Ranschaert, E., de Jong, P. A., Silva, M., Geurts, B., Chung, K., Schalekamp, S., Meersschaert, J., Devaraj, A., Pinsky, P. F., Lam, S. C., Ginneken, B. van, & Farahani, K. (2021). Deep Learning for Lung Cancer Detection on Screening CT Scans: Results of a Large-Scale Public Competition and an Observer Study with 11 Radiologists. *Radiology: Artificial Intelligence*, *3*(6), 210027.

Japanese Society of Radiological Technology (JSRT). (2026). JSRT Database. *JSRT Official Database Portal*.

Ji, L., Guo, Q., & Zhang, M. (2020). Medical Image Denoising Based on Biquadratic Polynomial With Minimum Error Constraints and Low-Rank Approximation. *IEEE Access*, *8*, 84950–84960. https://doi.org/10.1109/access.2020.2990463

Jian, M., Yu, X., Zhang, H., & Yang, C. (2024). SwinCT: feature enhancement based low-dose CT images denoising with swin transformer. *Multimedia Systems*, *30*(1), 1. https://doi.org/10.1007/s00530-023-01202-x

Jiang, B., Li, J., Lu, Y., Cai, Q., Song, H., & Lu, G. (2025). Eficient image denoising using deep learning: A brief survey. *Information Fusion*, *118*, 103013. https://doi.org/10.1016/j.inffus.2025.103013

Kang, B., Lee, W., Seo, H., Heo, H., & Park, H. (2024). Self-supervised learning for denoising of multidimensional MRI data. *Magnetic Resonance in Medicine*, *92*(5), 1980–1994. https://doi.org/10.1002/mrm.30197

Kidoh, M., Shinoda, K., Kitajima, M., Isogawa, K., Nambu, M., Uetani, H., Morita, K., Nakaura, T., Tateishi, M., Yamashita, Y., & Yamashita, Y. (2020). Deep Learning Based Noise Reduction for Brain MR Imaging: Tests on Phantoms and Healthy Volunteers. *Magnetic Resonance in Medical Sciences*, *19*(3), 195–206. https://doi.org/10.2463/mrms.mp.2019-0018

Kim, H.-J., & Lee, D. (2020). Image denoising with conditional generative adversarial networks (CGAN) in low dose chest images. *Nuclear Instruments and Methods in Physics Research Section A: Accelerators, Spectrometers, Detectors and Associated Equipment*, *954*, 161914. https://doi.org/10.1016/j.nima.2019.02.041

Kollem, S., Ramalinga Reddy, K., Srinivasa Rao, D., Rajendra Prasad, C., Malathy, V., Ajayan, J., & Muchahary, D. (2022). Image denoising for magnetic resonance imaging medical images using improved generalized cross-validation based on the diffusivity function. *International Journal of Imaging Systems and Technology*, *32*(4), 1263–1285. https://doi.org/10.1002/ima.22681

Kollem, S., Reddy, K. R., & Rao, D. S. (2021). Improved partial differential equation-based total variation approach to non-subsampled contourlet transform for medical image denoising. *Multimedia Tools and Applications*, *80*(2), 2663–2689. https://doi.org/10.1007/s11042-020-09745-1

Kollem, S., Reddy, K. R., & Rao, D. S. (2023). A novel diffusivity function-based image denoising for MRI medical images. *Multimedia Tools and Applications*, *82*(21), 32057–32089. https://doi.org/10.1007/s11042-023-14457-3

Krull, A., Buchholz, T.-O., & Jug, F. (2019). *Noise2Void - Learning Denoising From Single Noisy Images*. 2124–2132. https://doi.org/10.1109/cvpr.2019.00223

Laine, S., Karras, T., Lehtinen, J., & Aila, T. (2019). High-Quality Self-Supervised Deep Image Denoising. *Vancouver, Canada*, 6970–6980. https://doi.org/arXiv:1901.10277

Ledig, C., Theis, L., Huszar, F., Caballero, J., Cunningham, A., Acosta, A., Aitken, A., Tejani, A., Totz, J., Wang, Z., & Shi, W. (2017). Photo-Realistic Single Image Super-Resolution Using a Generative Adversarial Network. *2017 IEEE Conference on Computer Vision and Pattern Recognition (CVPR)*, 105–114. https://doi.org/10.1109/cvpr.2017.19

Lepcha, D. C., Dogra, A., Goyal, B., Goyal, V., Kukreja, V., & Bavirisetti, D. P. (2023a). A constructive non-local means algorithm for low-dose computed tomography denoising with morphological residual processing. *PLOS ONE*, *18*(9), e0291911. https://doi.org/10.1371/journal.pone.0291911

Lepcha, D. C., Goyal, B., & Dogra, A. (2023b). Image Matting: A Comprehensive Survey on Techniques, Comparative Analysis, Applications and Future Scope. *International Journal of Image and Graphics*, *23*(01), 2350011. https://doi.org/10.1142/s0219467823500110

Lepcha, D. C., Goyal, B., Dogra, A., & Goyal, V. (2023c). Image super-resolution: A comprehensive review, recent trends, challenges and applications. *Information Fusion*, *91*, 230–260. https://doi.org/10.1016/j.inffus.2022.10.007

Lepcha, D. C., Goyal, B., Dogra, A., Sharma, K. P., & Gupta, D. N. (2023d). A deep journey into image enhancement: A survey of current and emerging trends. *Information Fusion*, *93*, 36–76. https://doi.org/10.1016/j.inffus.2022.12.012

Leuschner, J., Schmidt, M., Baguer, D. O., & Maass, P. (2021). LoDoPaB-CT, a benchmark dataset for low-dose computed tomography reconstruction. *Scientific Data*, *8*(1). https://doi.org/10.1038/s41597-021-00893-z

Li, B., & Que, D. (2011). Medical Images Denoising Based on Total Variation Algorithm. *Procedia Environmental Sciences*, *8*, 227–234. https://doi.org/10.1016/j.proenv.2011.10.037

Li, S., Yin, H., & Fang, L. (2012). Group-Sparse Representation With Dictionary Learning for Medical Image Denoising and Fusion. *IEEE Transactions on Biomedical Engineering*, *59*(12), 3450–3459. https://doi.org/10.1109/tbme.2012.2217493

Li, Y., Zhang, K., Shi, W., Miao, Y., & Jiang, Z. (2021). A Novel Medical Image Denoising Method Based on Conditional Generative Adversarial Network. *Computational and Mathematical Methods in Medicine*, *2021*, 1–11. https://doi.org/10.1155/2021/9974017

Li, Z., Lu, S., Yuan, Z., Hou, B., & Bian, J. (2025). Interactive Instance Search: User-Centered Enhanced Image Retrieval with Learned Perceptual Image Patch Similarity. *Electronics*, *14*(9), 1766. https://doi.org/10.3390/electronics14091766

Liang, J., Cao, J., Sun, G., Zhang, K., Van Gool, L., & Timofte, R. (2021). SwinIR: Image Restoration Using Swin Transformer. *2021 IEEE/CVF International Conference on Computer Vision Workshops (ICCVW)*, 1833–1844. https://doi.org/10.1109/iccvw54120.2021.00210

Liu, C., Szeliski, R., Bing Kang, S., Zitnick, C. L., & Freeman, W. T. (2008). Automatic Estimation and Removal of Noise from a Single Image. *IEEE Transactions on Pattern Analysis and Machine Intelligence*, *30*(2), 299–314. https://doi.org/10.1109/tpami.2007.1176

Liu, P., El Basha, M. D., Li, Y., Xiao, Y., Sanelli, P. C., & Fang, R. (2019). Deep Evolutionary Networks with Expedited Genetic Algorithms for Medical Image Denoising. *Medical Image Analysis*, *54*, 306–315. https://doi.org/10.1016/j.media.2019.03.004

Liu, P., Li, Y., El Basha, M. D., & Fang, R. (2018). Neural Network Evolution Using Expedited Genetic Algorithm for Medical Image Denoising. *Published in Genetic and Evolutionary Computing: Proceedings of the 11th International Conference on Genetic and Evolutionary Computing (ICGEC 2017)*, 12–20. https://doi.org/10.1007/978-3-030-00928-1_2

Lu, K., He, N., & Li, L. (2012). Nonlocal Means-Based Denoising for Medical Images. *Computational and Mathematical Methods in Medicine*, *2012*(1), 438617. https://doi.org/10.1155/2012/438617

Luo, J., Zhu, Y., & Hiba, B. (2010). Medical image denoising using one-dimensional singularity function model. *Computerized Medical Imaging and Graphics*, *34*(2), 167–176. https://doi.org/10.1016/j.compmedimag.2009.08.007

Luthra, H. S., Mittal, T., Iyer, A., & Yadav, S. (2021). Eformer: Edge Enhancement based Transformer for Medical Image Denoising. *ArXiv Preprint*.

Mohan, M. R. M., Sulochana, C. H., & Latha, T. (2015). Medical image denoising using multistage directional median filter. *2015 International Conference on Circuits, Power and Computing Technologies [ICCPCT-2015]*. 2015 International Conference on Circuits, Power and Computing Technologies (ICCPCT), Nagercoil. https://doi.org/10.1109/iccpct.2015.7159261

Marcos, L., Babyn, P., & Alirezaie, J. (2024). Pure Vision Transformer (CT-ViT) with Noise2Neighbors Interpolation for Low-Dose CT Image Denoising. *Journal of Imaging Informatics in Medicine*, *37*(5), 2669–2687. https://doi.org/10.1007/s10278-024-01108-8

Ming, J., Yi, B., Zhang, Y., & Li, H. (2020). Low-dose CT Image Denoising Using Classification Densely Connected Residual Network. *KSII Transactions on Internet and Information Systems*, *14*(6), 2480–2496. https://doi.org/10.3837/tiis.2020.06.009

Mingliang, X., Pei, L., Mingyuan, L., Hao, F., Hongling, Z., Bing, Z., Yusong, L., & Liwei, Z. (2016). Medical image denoising by parallel non-local means. *Neurocomputing*, *195*, 117–122. https://doi.org/10.1016/j.neucom.2015.08.117

Miri, A., Sharifian, S., Rashidi, S., & Ghods, M. (2018). Medical image denoising based on 2D discrete cosine transform via ant colony optimization. *Optik*, *156*, 938–948. https://doi.org/10.1016/j.ijleo.2017.12.074

Moen, T. R., Chen, B., Holmes , D. R., Duan, X. D., Yu, Z., Yu, L., Leng, S., Fletcher, J. G., & McCollough, C. H. (2021). Low-dose CT image and projection dataset. *Med Phys*, *48*(2), 902–911.

Mohanapriya, G., Muthukumar, S., Santhosh, S. K., & Shanmugapriya, M. M. (2026). Kalman Bucy Filtered Neuro Fuzzy Image Denoising for Medical Image Processing. *Neutrosophic Sets and Systems*, *70*(1), 19.

Muksimova, S., Umirzakova, S., Mardieva, S., & Cho, Y.-I. (2023). Enhancing Medical Image Denoising with Innovative Teacher–Student Model-Based Approaches for Precision Diagnostics. *Sensors*, *23*(23), 9502. https://doi.org/10.3390/s23239502

Naimi, H., Adamou-Mitiche, A. B. H., & Mitiche, L. (2015). Medical image denoising using dual tree complex thresholding wavelet transform and Wiener filter. *Journal of King Saud University - Computer and Information Sciences*, *27*(1), 40–45. https://doi.org/10.1016/j.jksuci.2014.03.015

Nazir, N., Sarwar, A., & Saini, B. S. (2024). Recent developments in denoising medical images using deep learning: An overview of models, techniques, and challenges. *Micron*, *180*, 103615. https://doi.org/10.1016/j.micron.2024.103615

Rabbani, H., Nezafat, R., & Gazor, S. (2009). Wavelet-Domain Medical Image Denoising Using Bivariate Laplacian Mixture Model. *IEEE Transactions on Biomedical Engineering*, *56*(12), 2826–2837. https://doi.org/10.1109/tbme.2009.2028876

Rai, S., Bhatt, J. S., & Patra, S. K. (2021). An unsupervised deep learning framework for medical image denoising. *ArXiv*, arXiv:2103.06575.

Rajesh, C., & Kumar, S. (2022). An evolutionary block based network for medical image denoising using Differential Evolution. *Applied Soft Computing*, *121*, 108776. https://doi.org/10.1016/j.asoc.2022.108776

Rawat, S., Rana, K. P. S., & Kumar, V. (2021). A novel complex-valued convolutional neural network for medical image denoising. *Biomedical Signal Processing and Control*, *69*, 102859. https://doi.org/10.1016/j.bspc.2021.102859

Rudin, L. I., Osher, S., & Fatemi, E. (1992). Nonlinear total variation based noise removal algorithms. *Physica D: Nonlinear Phenomena*, *60*(1–4), 259–268.https://doi.org/10.1016/0167-2789(92)90242-f

Sagheer, M., S. V., & George, S. N. (2020). A review on medical image denoising algorithms. *Biomedical Signal Processing and Control*, *61*, 102036. https://doi.org/10.1016/j.bspc.2020.102036

Santos, L., Hsu, H.-Y., Nelson, R. R., Sullivan, B., Shin, J., Fung, M., Lebel, M. R., Jambawalikar, S., & Jaramillo, D. (2024). Impact of Deep Learning Denoising Algorithm on Diffusion Tensor Imaging of the Growth Plate on Different Spatial Resolutions. *Tomography*, *10*(4), 504–519. https://doi.org/10.3390/tomography10040039

Satheesh, S., & Prasad, K. V. S. V. R. (2011). Medical Image Denoising Using Adaptive Threshold Based on Contourlet Transform. *Advanced Computing: An International Journal*, *2*(2), 52–58. https://doi.org/10.5121/acij.2011.2205

Sharif, S. M. A., Naqvi, R. A., & Biswas, M. (2020). Learning Medical Image Denoising with Deep Dynamic Residual Attention Network. *Mathematics*, *8*(12), 2192. https://doi.org/10.3390/math8122192

Sharif, S. M. A., Naqvi, R. A., & Loh, W.-K. (2024). Two-Stage Deep Denoising With Self-Guided Noise Attention for Multimodal Medical Images. *IEEE Transactions on Radiation and Plasma Medical Sciences*, *8*(5), 521–531. https://doi.org/10.1109/trpms.2024.3380090

Shivahare, B. D., Gupta, S. K., Katiyar, A. N., S., P., Singh, P., & Diwakar, M. (2023). Medical Image Denoising and Brain Tumor Detection Using CNN and U-Net. *2023 3rd International Conference on Innovative Sustainable Computational Technologies (CISCT)*. 2023 3rd International Conference on Innovative Sustainable Computational Technologies (CISCT), Dehradun, India. https://doi.org/10.1109/cisct57197.2023.10351338

Shung, K. K., Smith, M., & Tsui, B. M. W. (2012). *Principles of medical imaging*.

Sidhu, K. S., Khaira, B. S., & Virk, I. S. (2012). Medical Image Denoising In the Wavelet Domain Using Haar And DB3 Filtering. *International Refereed Journal of Engineering and Science (IRJES)*, *1*(2), 30–36.

Singh, P., Diwakar, M., Pandey, N. K., Singh, R., Sisodia, D., Arya, C., & Chakraborty, C. (2023). Low-dose COVID-19 CT Image Denoising Using CNN and its Method Noise Thresholding. *Current Medical Imaging Reviews*, *19*(2), 182–193. https://doi.org/10.2174/1573405618666220404162241

Singh, P., Singh, R., Singh, S., Singh, R., & Kumar, R. (2022). A Method Noise-Based Convolutional Neural Network Technique for CT Image Denoising. *Electronics (Switzerland*, *11*(21), 3535. https://doi.org/https://doi.org/10.3390/electronics11213535

Song, Q., Li, X., Zhang, M., Zhang, X., & Thanh, D. N. H. (2024). APNet: Adaptive projection network for medical image denoising. *Journal of X-Ray Science and Technology: Clinical Applications of Diagnosis and Therapeutics*, *32*(1), 1–15. https://doi.org/10.3233/xst-230181

Swetha, D., & Jyothi, N. (2025). Medical Image Denoising Using a Novel Multilevel Convolutional Optimized Visual Attention Network in Diverse Dataset. *International Journal of Image and Graphics*, *14*. https://doi.org/10.1142/s0219467827500252

Taassori, M. (2024). Enhanced Wavelet-Based Medical Image Denoising with Bayesian-Optimized Bilateral Filtering. *Sensors*, *24*(21), 6849. https://doi.org/10.3390/s24216849

Taassori, M., & Vizvári, B. (2024). Enhancing Medical Image Denoising: A Hybrid Approach Incorporating Adaptive Kalman Filter and Non-Local Means with Latin Square Optimization. *Electronics*, *13*(13), 2640. https://doi.org/10.3390/electronics13132640

Thielemans, K., Tsoumpas, C., Mustafovic, S., Beisel, T., Aguiar, P., Dikaios, N., & Jacobson, M. W. (2012). STIR: software for tomographic image reconstruction release 2. *Physics in Medicine and Biology*, *cc*(4), 867–883. https://doi.org/10.1088/0031-9155/57/4/867

Upadhyay, U., Chen, Y., & Akata, Z. (2021). Uncertainty-aware generalized adaptive CycleGAN. *arXiv preprint arXiv:2102.11747*. https://doi.org/10.48550/arXiv.2102.11747

Vaiyapuri, T., Alaskar, H., Sbai, Z., & Devi, S. (2021). GA-based multi-objective optimization technique for medical image denoising in wavelet domain. *Journal of Intelligent and Fuzzy Systems*, *41*(1), 1575–1588. https://doi.org/10.3233/jifs-210429

Vincent, P., Larochelle, H., Bengio, Y., & Manzagol, P.-A. (2008). Extracting and composing robust features with denoising autoencoders. *Proceedings of the 25th International Conference on Machine Learning - ICML '08*, 1096–1103. https://doi.org/10.1145/1390156.1390294

Wang, X., Peng, Y., Lu, L., Lu, Z., Bagheri, M., & Summers, R. M. (2017). ChestX-Ray8: Hospital-Scale Chest X-Ray Database and Benchmarks on Weakly-Supervised Classification and Localization of Common Thorax Diseases. *2017 IEEE Conference on Computer Vision and Pattern Recognition (CVPR)*, 3462–3471. https://doi.org/10.1109/cvpr.2017.369

Wang, Y., & Zhou, H. (2006). Total Variation Wavelet-Based Medical Image Denoising. *International Journal of Biomedical Imaging*, *2006*(1), 089095. https://doi.org/10.1155/ijbi/2006/89095

Wang, Z., Bovik, A. C., Sheikh, H. R., & Simoncelli, E. P. (2004). Image Quality Assessment: From Error Visibility to Structural Similarity. In *IEEE Transactions on Image Processing* (Vol. 13, Issue 4, pp. 600–612). https://doi.org/10.1109/tip.2003.819861

Wu, W., Chen, M., Xiang, Y., Zhang, Y., & Yang, Y. (2023). Recent progress in image denoising: A training strategy perspective. *Science and Technology*, *17*(6), 1367–1383.

Xu, J., & Adalsteinsson, E. (2021). Deformed2Self: Self-supervised Denoising for Dynamic Medical Imaging. *Medical Image Computing and Computer*, *12902*, 25–35. https://doi.org/10.1007/978-3-030-87196-3_3

Xu, X., Xu, C., & Zhao, L. (2025). Real-Time Volume-Rendering Image Denoising Based on Spatiotemporal Weighted Kernel Prediction. *Journal of Imaging*, *11*(4), 126. https://doi.org/10.3390/jimaging11040126

Yan, K., Wang, X., Lu, L., & Summers, R. M. (2018). DeepLesion: automated mining of large-scale lesion annotations and universal lesion detection with deep learning. *Journal of Medical Imaging*, *5*(3), 036501. https://doi.org/10.1117/1.jmi.5.3.036501

Yang, J., & Shi, R. (2026). MedMNIST: Standardized Biomedical Images. *Kaggle Datasets (Hosted by Kaggle, Google LLC)*.

Yuan, J., Zhou, F., Guo, Z., Li, X., & Yu, H. (2023). HCformer: Hybrid CNN-Transformer for LDCT Image Denoising. *Journal of Digital Imaging*, *36*(5), 2290–2305. https://doi.org/10.1007/s10278-023-00842-9

Zbontar, J., Knoll, F., Sriram, A., Murrell, T., Huang, Z., J. Muckley, M., Defazio, A., Stern, R., Johnson, P., Bruno, M., Parente, M., Geras, K. J., Katsnelson, J., Chandarana, H., Zhang, Z., Drozdzal, M., Romero, A., Rabbat, M., Vincent, P., & Lui, Y. W. (2018). fastMRI: An Open Dataset and Benchmarks for Accelerated MRI. *ArXiv*.

Zeng, X., Guo, Y., Li, L., & Liu, Y. (2024). Continual medical image denoising based on triplet neural networks collaboration. *Computers in Biology and Medicine*, *179*, 108914. https://doi.org/10.1016/j.compbiomed.2024.108914

Zhang, K., Zuo, W., Chen, Y., Meng, D., & Zhang, L. (2017). Beyond a Gaussian Denoiser: Residual Learning of Deep CNN for Image Denoising. *IEEE Transactions on Image Processing*, *26*(7), 3142–3155. https://doi.org/10.1109/tip.2017.2662206

Zhao, H., Gallo, O., Frosio, I., & Kautz, J. (2017). Loss Functions for Image Restoration With Neural Networks. *IEEE Transactions on Computational Imaging*, *3*(1), 47–57. https://doi.org/10.1109/tci.2016.2644865

Zhao, W., & Lu, H. (2017). Medical Image Fusion and Denoising with Alternating Sequential Filter and Adaptive Fractional Order Total Variation. *IEEE Transactions on Instrumentation and Measurement*, *66*(9), 2283–2294. https://doi.org/10.1109/tim.2017.2700198

Zhou, L., Schaefferkoetter, J. D., Tham, I. W. K., Huang, G., & Yan, J. (2020). Supervised learning with cyclegan for low-dose FDG PET image denoising. *Medical Image Analysis*, *65*, 101770. https://doi.org/10.1016/j.media.2020.101770